Heterogeneous oxidation of amorphous organic aerosol surrogates by O_3, NO_3, and OH at typical tropospheric temperatures

Jienan Li, Seanna M. Forrester, Daniel A. Knopf

5 School of Marine and Atmospheric Sciences, Stony Brook University, Stony Brook, NY 11794-5000, USA

Correspondence to: Daniel A. Knopf (Daniel.knopf@stonybrook.edu)

Abstract. Typical tropospheric temperatures render possible phase states of amorphous organic aerosol (OA) particles to solid, semi-solid and liquid. This will affect the multiphase oxidation kinetics involving the organic condensed phase and gaseous
10 oxidants and radicals. To quantify this effect, we determined the reactive uptake coefficients (γ) of O_3, NO_3 and OH by substrate films composed of single and binary OA surrogate species under dry conditions for temperatures from 213 to 313 K. A temperature-controlled coated-wall flow reactor coupled to a chemical ionization mass spectrometer was applied to determine γ with consideration of gas diffusion transport limitation and gas flow entrance effects, which can impact heterogeneous reaction kinetics. The phase state of the organic substrates was probed via the poke-flow technique, allowing
15 the estimation of the substrates' glass transition temperatures. γ values for O_3 and OH uptake to a canola oil substrate, NO_3 uptake to a levoglucosan and a levoglucosan/xylitol substrate, and OH uptake to a glucose and glucose/1,2,6-hexanetriol substrate have been determined as a function of temperature. We observed the greatest changes in γ with temperature for substrates that experienced the largest changes in viscosity as a result of a solid-to-liquid phase transition. Organic substrates that maintain a semi-solid or solid phase state and as such a relatively higher viscosity, do not display large variations in
20 heterogeneous reactivity. From 213 K to 293 K, γ values of O_3 with canola oil, of NO_3 with a levoglucosan/xylitol mixture, and of OH with a glucose/1,2,6-hexanetriol mixture and canola oil, increase by about a factor of 34, 3, 2 and 5, respectively, due to a solid-to-liquid phase transition of the substrate. These results demonstrate that the surface and bulk lifetime of the OA surrogate species can significantly increase due to the slowed heterogeneous kinetics when OA species are solid or highly viscous in the middle and upper troposphere. This experimental study will further our understanding of the chemical evolution
25 of OA particles with subsequent important consequences for source apportionment, air quality, and climate.

1 Introduction

Organic aerosol (OA) particles are ubiquitous and can represent 20%-90% of the mass fraction of the submicron aerosol (particles ≤ 1 μm in diameter) in the atmosphere. The significance of OA has long been established, influencing air quality, human health, cloud formation process and the radiative budget, on a regional and global scale, and thus climate (Hallquist et
30 al., 2009;Jimenez et al., 2009;Seinfeld and Pandis, 2016;Stocker et al., 2013;Knopf et al., 2018;Abbatt et al., 2019;Shiraiwa et

al., 2017b;Kanakidou et al., 2005;Pachauri et al., 2014;Pöschl and Shiraiwa, 2015). Characterizing these impacts crucially depends on our ability to determine and quantify aerosol sources and strengths (Bai et al., 2013;Robinson et al., 2006;McFiggans et al., 2019;Hopke, 2016), and to understand the physical and chemical transformation of aerosol particles during atmospheric transport by multiphase chemical processes (George and Abbatt, 2010;Rudich et al., 2007;Laskin et al.,
35   2015;Springmann et al., 2009;Kaiser et al., 2011;Ervens et al., 2011;Zhou et al., 2019;Moise et al., 2015). Gas-to-particle, also termed heterogeneous, reactions can involve organic components in the condensed phase and gas-phase oxidants such as O_3, NO_3, and OH. These reactions, which can include multiple phases, change the physicochemical properties of particles including composition, density, and hygroscopicity, thereby defining their chemical lifetime, optical properties, and ice nucleating ability (Jimenez et al., 2009;Kroll et al., 2015;Katrib et al., 2005b;Knopf et al., 2018;Slade et al., 2017;Robinson et al., 2007;Shiraiwa
40   et al., 2017a;Moise et al., 2015;Shiraiwa et al., 2012).

It is now well established that OA can exhibit amorphous phase states (Mikhailov et al., 2009;Virtanen et al., 2010;Koop et al., 2011;Reid et al., 2018). Depending on the viscosity and microstructure, the amorphous phases can be classified as glasses, rubbers, gels, or ultra-viscous liquids (Mikhailov et al., 2009;Riemer et al., 2019). The glass transition temperature, T_g, is a characteristic parameter to describe the viscosity of a liquid on the order of 10^{12} Pa s (Koop et al., 2011;Angell, 1995;Zobrist
45   et al., 2011). At this temperature, the molecular motion of the species is so slow that it can be considered a solid. The phase state of OA can be modulated by particle composition and environmental conditions such as relative humidity (RH) and temperature (Koop et al., 2011;Zobrist et al., 2008;Shiraiwa et al., 2017a;Petters et al., 2019). Particle viscosity will influence the diffusion of atmospheric oxidants and other small gas molecules (e.g., O_3, OH, NO_3, H_2O) entering the organic matrix (Price et al., 2015;Zobrist et al., 2011;Slade et al., 2017;Davies and Wilson, 2016;Moridnejad and Preston, 2016) as well as
50   the transport and mixing of the condensed-phase organic species (Rothfuss and Petters, 2017;Marsh et al., 2018;Lienhard et al., 2015;Abramson et al., 2013;Chenyakin et al., 2017;Kiland et al., 2019). Therefore, it can be expected that the particle phase state will significantly affect the rate of multiphase chemical kinetics (Shiraiwa and Seinfeld, 2012;Slade and Knopf, 2014;Kolesar et al., 2014;Knopf et al., 2005;Katrib et al., 2005a;Davies and Wilson, 2015;Pöschl and Shiraiwa, 2015). The heterogeneous reaction kinetics are often expressed by the reactive uptake coefficient (γ), which represents the fraction of gas
55   collisions with a substrate surface that yield uptake or reaction (Pöschl et al., 2007;Schwartz, 1986).

As has been demonstrated for heterogeneous ozonolysis reactions, the composition of the condensed phase can alter the phase state, thereby, significantly altering the reactive uptake kinetics (Knopf et al., 2005;Hearn et al., 2005;de Gouw and Lovejoy, 1998;Ziemann, 2005). In general, the solid condensed phase showed significantly lower γ_{O_3} values compared to the ozonolysis of the liquid phase. Recent experimental studies focused on how relative humidity (RH) influences the reactive
60   uptake of gas oxidants via its impact on the phase state of the organic species (Berkemeier et al., 2016;Steimer et al., 2015;Shiraiwa et al., 2011;Slade and Knopf, 2014;Li et al., 2018;Davies and Wilson, 2015;Hu et al., 2016;Marshall et al., 2018). The heterogeneous oxidation of a typical component of biomass burning aerosol (BBA) particles, levoglucosan (LEV) by OH yielded γ values in the range from 0.008 to 1 with implications for the lifetime of LEV ranging from weeks at dry conditions (Slade and Knopf, 2013;Kessler et al., 2010;Slade and Knopf, 2014) to a couple of days when LEV is in a more

65   liquid-like state in response to ambient RH (Yang et al., 2013;Bai et al., 2013;Slade and Knopf, 2014). The general conclusion is that at lower RH, the reactive uptake can be dominated by surface reactions when the condensed phase is in a solid state, whereas at higher RH, the condensed phase can be semi-solid or liquid and the oxidation process can commence at the surface and in the bulk. For the latter scenario, the gaseous oxidants can access greater depths of the condensed phase, and the oxidized organic species at the surface can be readily replenished by unreacted molecules from the bulk (Arangio et al., 2015;Slade and

70   Knopf, 2014). Davies and Wilson (2015) investigated how the viscosity change of citric acid, due to changes in water content, governs the reactive uptake of OH radicals. They observed that the depletion of citric acid and the formation of reaction products are confined near the aerosol-gas interface on the order of 8 nm at 20% RH, and the reaction depth increases to ~50 nm at 50% RH. Recently, Li et al. (2018) observed that the heterogeneous aging of SOA by OH radicals at 89% RH and 25% RH resulted in ~60% and 20% loss of particle mass, respectively. The authors concluded that this difference in particle mass

75   degradation is attributed to a larger OH uptake coefficient and/or larger fragmentation probability at higher RH.

        The temperature in the troposphere ranges approximately from 200 K to 300 K (Wallace and Hobbs, 2006), with subsequent impact on the OA phase state (Shiraiwa et al., 2017a;Koop et al., 2011) and multiphase reaction kinetics. However, only a few laboratory studies investigated the temperature dependence of heterogeneous oxidation reactions while considering the phase transition of organic substrates and aerosol particles (de Gouw and Lovejoy, 1998;Edebeli et al., 2019;Gross et al.,

80   2009;Knopf et al., 2005;Moise and Rudich, 2002;Slade et al., 2017;Moise and Rudich, 2000;Moise et al., 2002). Moise and Rudich (2002) demonstrated that the uptake of ozone by oleic and linoleic acid is a strong function of temperature, where γ decreases by about an order of magnitude with decreasing temperature when both substrates transformed from a liquid to a solid state. Similarly, Gross et al. (2009) observed a decrease of 70% to 90% for γ of NO_3, as oleic acid, diethyl sebacate, and conjugated linoleic acid substrates solidified as the temperature decreased from 302 K to 263 K. The authors suggested that

85   the net liquid phase reaction involves both a surface reaction and a bulk reaction, whereas solidification of the substrate greatly minimizes the significance of any bulk reactions. This is in line with results of a kinetic flux model applied to NO_3 exposure studies of solid LEV and abietic acid substrates, further indicating that under shorter time scales reactive uptake was dominated by surface reaction, whereas for times scales greater than ~100 s, even for a solid organic substrate, bulk processes can impact the overall reactive uptake kinetics (Shiraiwa et al., 2012). Very recently, Edebeli et al. (2019) investigated the temperature

90   dependence of bromide oxidation by ozone in a citric acid/bromide mixture and observed that γ decreases from 2×10^{-6} at 289 K to 0.5×10^{-6} at 245 K. Their analysis indicated that the humidity-driven acceleration in uptake reactivity decreased due to the increased viscosities of the citric acid/bromide mixture and decreased diffusivity of ozone as the temperature was lowered. The effect of temperature on uptake kinetics via its impact on the condensed phase state has also been highlighted in a recent modeling study (Mu et al., 2018), which showed that low temperature conditions can substantially increase the lifetime of

95   PAHs against O_3 and enhance their dispersion through both the planetary boundary layer and the free troposphere. Temperature also impacts the other processes involved in multiphase kinetics (Schwartz, 1986;Pöschl et al., 2007), including the collision flux of gas-phase species, the desorption rate and surface and bulk reaction rates, both typically expressed by an Arrhenius factor (Laidler et al., 1940;Pöschl et al., 2007;Baetzold and Somorjai, 1976). Clearly, the temperature dependency of the

reaction kinetics and the role of the condensed phase state pose a challenge for detangling the underlying physicochemical

100 processes governing multiphase chemical kinetics of OA under typical tropospheric conditions.

To add to our understanding of multiphase chemical kinetics at low temperatures, we determined the reactive uptake of O_3, NO_3 and OH by OA surrogates for temperatures ranging from 213 K to 293 K under dry conditions. We employed a chemical ionization mass spectrometer coupled to a coated-wall flow-tube reactor. As OA proxies, we applied substrates of canola oil (CA), levoglucosan (LEV), a levoglucosan/xylitol mixture (LEV/XYL), glucose (GLU), and a glucose/1,2,6-

105 hexanetriol mixture (GLU/HEX). Some of the examined substrates undergo a phase transition from liquid to solid in the probed temperature regime with subsequent consequences for the heterogeneous uptake kinetics. The substrate's phase state was qualitatively verified by conducting film poke-flow experiments. The results of our reactive uptake experiments emphasize the importance of the temperature-induced phase changes of the OA surrogates when describing the chemical degradation of OA during atmospheric transport.

110 **2 Experimental methods**

2.1 Apparatus

The experimental system is based on our previous setups (Slade and Knopf, 2013;Knopf et al., 2011;Knopf et al., 2005) and includes a temperature-controlled coated-wall flow reactor and a custom-built chemical ionization mass spectrometer (CIMS), as shown in Fig. 1. It consists of three parts: gas-phase oxidant generation, multiphase chemical reaction, and oxidant detection.

115 The gas-phase oxidant (O_3, NO_3, or OH) enters the coated-wall flow reactor via a movable injector, where it can react with the organic substrate film coating on the inner wall of a rotating tube. The changes in oxidant concentration are measured by CIMS via soft ionization in the chemical ionization region.

The uptake measurements are conducted in a temperature range of 213 to 313 K. The axial temperature variation in the flow reactor is smaller than 1 K for all our experimental conditions, which is determined with a thermocouple that is fixed at

120 the tip of the injector, as discussed in the Supplement S1. The rotating tube fits snuggly inside the flow tube that is enclosed by a cooling jacket for temperature control. The rotating speed of the substrate tube is set to ~5-10 rpm to keep the liquid film evenly distributed on its inner surface. The pressure in flow reactor ranges from 2 to 5 hPa depending on the applied oxidant gases.

For OH radical uptake experiments, an additional rotary pump is directly connected to the flow reactor. The pump is

125 used to lower the flow reactor pressure to < 2.5 hPa, thus minimizing gas transport limitation due to diffusion (Knopf et al., 2015;Zasypkin et al., 1997) while simultaneously maintaining a high flow rate. Two sizes of rotating glass cylinders with diameters of 1.75 cm and 1.2 cm are used in these uptake experiments. The latter one is designed specifically for OH heterogeneous reactions to avoid limitation of gas transport by diffusion. For O_3 and NO_3 uptake experiments, gas transport limitations due to diffusion can be neglected under applied flow conditions because of a slower reactive uptake.

130   The pseudo-first-order loss of the oxidant species to the organic substrate is determined by monitoring the loss of the gaseous oxidants as the injector is pulled back in 1 or 2 cm increments until reaching 10 cm. The flow rate of gas oxidants in the movable injector ranges from 2 to 100 $cm^3 min^{-1}$ STP (standard temperature and pressure). The flow rate of the carrier gas He in the flow reactor ranges from 30 to 900 $cm^3 min^{-1}$ STP. As a result, the residence time varies two orders of magnitude in these experiments, ranging from ~2 ms for OH uptake to 100 ms for O_3 uptake. The Reynolds number (Re) for all experiments

135   is below 20, indicating laminar flow conditions. Care has been taken to ensure a carrier-to-injector gas velocity ratio of >1.33, in order to avoid the disruption of the gas flow by a fast gas flow exiting the injector, as pointed out by Davis (2008). This condition is also a necessity to accurately account for the gas flow entrance effect, which is important for fast uptake kinetics, as further discussed in the Appendix. The γ value at each temperature reported in this study is derived from at least 6 reactive uptakes, with a freshly prepared organic substrate employed for each.

2.2 Oxidant formation, detection and flow conditions

140   A carbon filter (Supelco, Superlcarb HC) and a Drierite cold trap cooled with liquid nitrogen or an ethanol/dry ice mixture are used to purify ultra-high purity (UHP) gases of N_2, He and O_2. O_3 is generated by introducing a flow of O_2 through a UV source (Jelight, model #600) prior to the injector. The flow rate of the O_2/O_3 mixture ranged between 2 - 7 $cm^3 min^{-1}$ (STP). A carrier He gas flow of 30-85 $cm^3 min^{-1}$ (STP) enters the flow reactor, mixes with the injector O_2/O_3 gas flow, and results in a

145   laminar flow with Re < 3. O_3 is detected as O_3^- after charge transfer reaction with SF_6^-. SF_6^- is generated by passing a minor amount of SF_6 in $N_2(g)$ through a ^{210}Po source. The O_3 concentrations ranged between 1.5×10^{11} - 2.1×10^{12} molecules cm^{-3}, reflecting typical atmospheric concentrations (Wallace and Hobbs, 2006;Finlayson-Pitts and Pitts Jr, 1999).

    NO_3 is generated by thermal dissociation of N_2O_5 gas at 433 K in a glass oven prior to the injector, as previously (Knopf et al., 2006;Knopf et al., 2011). N_2O_5 is generated via reaction of NO_2 and O_3 and stored as pure N_2O_5 crystals in a glass

150   container at 193 K. A gas flow of N_2O_5 in He of about 12-18 $cm^3 min^{-1}$ STP is further diluted by 100-120 $cm^3 min^{-1}$ (STP) He(g) flow before entering the injector. The flow reactor carrier gas is composed of He and O_2 at ~500 and ~100 $cm^3 min^{-1}$ (STP), respectively. This results in laminar flow conditions (Re < 10). NO_3 is detected as NO_3^- after chemical ionization by I^-. NO_3 concentrations are obtained via titration of a known amount of NO, resulting in 8×10^9 to 7×10^{11} molecules cm^{-3}, representing typical atmospheric NO_3 nighttime concentrations (Finlayson-Pitts and Pitts Jr, 1999;Brown et al., 2006)

155   OH radicals are produced following previously established methods (Bertram et al., 2001;Slade and Knopf, 2014) via the reaction of H atoms with O_2. A 2.45 GHz Evenson microwave cavity powered by a microwave generator is utilized to maintain an H plasma. The H atoms are formed by flowing a mixture of $H_2(g)$ (1-2 $cm^3 min^{-1}$, STP) and He(g) (40-80 $cm^3 min^{-1}$, STP) through a 1/4" OD (outer diameter). Pyrex tube that runs through the center of the microwave cavity. The generated H atoms then pass through a 1/8" OD. Pyrex tube directed down the center of a 1/4" OD Pyrex injector where OH production occurs

160   with H radicals reacting with $O_2(g)$ at 2-22 $cm^3 min^{-1}$ (STP). Complete reaction to OH is ensured by monitoring the formation of OH^- via charge transfer with SF_6^- in the CIMS. At colder flow reactor temperatures, the usable injector length is shortened to avoid artifacts in OH concentration due to temperature gradients in the injector tube which can impact OH formation

(Atkinson et al., 2004). A He gas flow of 700-900 cm^3 min^{-1} (STP) enters the flow reactor and further mixes with the injector flow, yielding a laminar gas flow with Re < 20. Employed OH concentrations ranged between 5×10^7 and 1×10^9 molecule cm^{-3}, which are higher than typical background OH concentrations of 10^6 molecule cm^{-3} (Finlayson-Pitts and Pitts Jr, 1999).

2.3 Substrate film preparation and characterization

The film substrate preparation method when using a coated-wall flow reactor has been discussed in detail in previous studies (Knopf et al., 2011;Slade and Knopf, 2013). Canola oil is liquid and thus can be directly applied on the inner surface of the rotating tube. The other organic substrates, i.e., LEV, LEV/XYL mixture, GLU and GLU/HEX mixture, are first dissolved in water and then 1-2 ml of the aqueous solution is evenly distributed inside the rotating glass tube. The concentration of the LEV solution is 5% (w/w) due to its relatively lower solubility, and all other solutions are 10% (w/w). The organic mass ratios of the LEV/XYL and GLU/HEX films are 1:1 and 4:1, respectively. As outlined further below, these mass ratios were chosen to set the expected glass transition temperature within the examined temperature range. During the entire process, a dry He or N$_2$ purging gas flow is applied to avoid contamination by room air. The glass tube is rotating in the flow reactor until a smooth coating is established. To dry the substrate, the substrate is exposed to rough vacuum conditions (1~2 hPa) resulting in the evaporation of water. Surface solidification of single-component saccharide films may result in trapping of condensed-phase water and thus impacting the film composition and its viscosity. The remaining water content for all substrate films after the drying process were determined to be 10% -16% (w/w) by measuring the mass change of the organic substrate films before and after the drying process with an ultra-microbalance (Mettler Toledo XP2U), as detailed in Supplement S2. The thickness of the applied organic film is estimated to be around 50-100 µm. We assume a smooth surface morphology and use the geometric surface area of the film to derive γ.

The phase state of the applied organic substrates at different temperatures can be qualitatively verified by using the poking experiments outlined below. The "poke-flow" technique has been applied to quantitatively estimate the viscosity of amorphous organic particles (Murray et al., 2012) including secondary organic material (SOM) produced by α-pinene ozonolysis (Renbaum-Wolff et al., 2013). A similar setup is used here to qualitatively investigate the phase state of applied amorphous substrates at different temperatures ranging from 213 to 313 K. A temperature-controlled cooling stage (Linkam BSC 196) is coupled to an optical microscope (Olympus BX51) (Fig. 2). The organic film substrate, generated from a volume of 2 µl liquid applied to a glass slide, is first placed into the flow reactor, undergoing the same preparation method as the substrate films employed for reactive uptake experiments. This results in a film with a thickness of about 50-100 µm. The substrate film is then moved into the poke-flow experiment. In the cooling stage the organic film sample is sealed against room air during the entire poking process. After poking with a needle, the phase states and flow characteristics of the organic substrate films at different temperatures are determined under the microscope as a function of time. The calibration of the cooling stage was performed via measurements of the melting points of octane (216.35 K), decane (243.5 K) and water (273.15 K). Before each experiment, the temperature was verified by measuring the melting temperature of three 2 µL water droplets (273.15 K). The

195 difference to the expected melting temperature difference is always smaller than 1 °C. We measured T_g with at least five independently prepared substrate films.

2.4 Chemicals

Listed below are the chemicals we used in our study, and corresponding purities and manufactures. N_2 (ultra-high purity, UHP), O_2 (UHP), H_2 (UHP) and He (UHP) were purchased from Airgas East. SF_6 (99.998%) was acquired from Praxair. NO_2 (99.5%)

200 was purchased from Mathenson. 1,6-anhydro-b-D-glucopyranose (99%) was purchased from Acros Organics. Glucose (99%) and xylitol (99%) were acquired from Alfa Aesar. 1,2,6-Hexanetriol (96%) and iodomethane (99%) were purchased from Sigma-Aldrich. Purity of canola oil was not determined. Millipore water (resistivity >18.2 MΩ cm) was applied to prepare aqueous solutions for generation of organic substrates.

3 Results and Discussion

205 ### 3.1 Characterization of substrate phase state

Images of the film surfaces in Fig. 3 show the flow characteristics and the morphologies of a GLU/HEX substrate mixture when subject to poking by a needle. In the experiment at $T = 293$ K (Fig. 3A), the film surface is deformed after being poked, leaving a black dent. The film flowed at an observable rate to restore a smooth surface, minimizing the surface energy of the system (Fig. 3A). At 273 K, the same deformed film did not show observable changes within 30 minutes (Fig. 3B). Only after

210 8 hours, minor changes in film morphology can be identified, clearly demonstrating greater substrate viscosity at this temperature compared to 293 K. At 253 K, the notch by poking on the surface maintains its shape for 8 hours, indicative of a semi-solid phase state (Fig. 3C). At $T = 233$ K, which is below the predicted $T_g = 248$ K, the surface shattered when poked with a needle (Fig. 3D). Furthermore, over the experimental observation time of 8 h, no restorative flow was observed at 233 K. The fragments have clear glass-like cracks, and no smoothing of the edges was observed over the course of the experiment.

215 Based on our poke-flow experiments as shown in Figure S2-S7, the applied GLU and LEV substrates remain in a solid or semi-solid phase state within the temperature range of 213 K to 313 K. However, the mixtures of GLU/HEX and LEV/XYL exist as liquids at 293 K and experience a glass phase transition with decreasing temperature.

By monitoring the substrate surface morphology, we can estimate T_g of the applied substrates as the highest temperature when shattering occurs. All images of the poke-flow experiment are documented in Figs. S2-S7 in the Supplement S3. Table

220 1 gives the estimated T_g^{exp} values of applied substrates compared to literature T_g^{lit} and predicted T_g^{pred} values. T_g^{pred} is derived from the Gordon Taylor equation (Gordon and Taylor, 2007) assuming no residual water in the organic mixture. Since T_g determination depends on cooling or drying rates, we do not expect agreement with literature values or predicted values. For most investigated substrates, our estimated T_g^{exp} is lower than either T_g^{lit} or T_g^{pred}. This is consistent with the notion that our substrates contain some residual water that lowers T_g.

225

The temperature dependence of the substrate viscosity can be predicted by using the modified Vogel-Tammann-Fulcher (VTF) equation (Angell, 1991):

$$\log \eta = -5 + 0.434 \frac{T_0 D}{T - T_0} \ , \tag{1}$$

where T_0 is the Vogel temperature and T is the ambient temperature. The fragility parameter, D, is defined in terms of the

230   deviation of the temperature dependence of the viscosity from the simple Arrhenius behavior. Assuming $T = T_g$, $\eta = 10^{12}$ Pa s, T_0 can be represented by T_g (DeRieux et al., 2018):

$$T_0 = \frac{39.17 T_g}{D + 39.17} \ . \tag{2}$$

Therefore, the temperature dependence of substrate viscosity can be predicted using our measured T_g^{exp} as illustrated in Fig. 4. For our calculations, we use literature D values for pure sugars and a mass-weighted interpolation of D values for the

235   mixtures as shown in Table 1. In Fig. 4a, LEV maintains a relatively higher viscosity compared to the LEV/XYL mixture throughout the studied temperature. The poke-flow experiments indicate the presence of a liquid phase at 293 K and solid phase at 238 K. In contrast to our poke-flow experiments, Fig. 4a suggests that the LEV/XYL mixture does not show a liquid phase in the examined temperature regime. Capturing this phase transition with the modified VTF equation (Angell , 1991), can be only achieved when using lower D values of 5.7~7.6 (compared to the interpolated D value of the LEV/XYL mixture),

240   a reasonable assumption when considering the presence of residual water in the substrate. The addition of water increases the steepness of the glass transition and decreases D values by potentially reducing the thermal energy necessary to promote the cooperative chain motions (Angell, 2002;Borde et al., 2002). Furthermore, a study of the trehalose/water system corroborates that the presence of water lowers D values to 3.32 - 4.85 as a lower limit (Elias and Elias, 1999). For GLU and the GLU/HEX mixture shown in Fig. 4b, adding HEX to GLU greatly lowers the T_g of the mixture, and thus decreases its viscosity. Also, in

245   this case, the predicted substrate viscosity of GLU/HEX disagrees with our observations when interpolating the D values of the pure compounds. A D value between 4.3 and 5.7 better represents the observed phase transition of the GLU/HEX mixture.

3.2 Reactive uptake kinetics

The uptake coefficient is determined experimentally from the loss of the gas phase oxidant to the organic substrate as the substrate area or corresponding reaction time is changed. Figure 5 shows three exemplary uptakes of O_3 by the canola oil (CA)

250   film, NO_3 by LEV film and OH radical by the GLU film, indicating the stepwise irreversible removal of the gas oxidants. Taking O_3 uptake as an example, the injector is pulled back in 2 cm increments until reaching 10 cm and is then pushed back to its original position (0 cm), with normalized O_3 signals recovering to unity.

From these data, the observed first-order wall loss rate, k_{obs}, is determined as the slope of the change in the natural logarithm of the oxidant signal as a function of reaction time, i.e., the residence time of the oxidants in the flow reactor (Knopf

255   et al., 2011;Slade and Knopf, 2013). Figure 6 shows exemplary k_{obs} derived for uptakes of O_3, NO_3, and OH for various

temperatures. k_{obs} is obtained from the slope of the linear fit to the data. The good linear regression indicates that the reported uncertainties for γ are likely due to the variability of organic substrates and uncertainty in the diffusion coefficient. In the case of O$_3$ uptake (Fig. 6a), we can identify two different regimes of k_{obs}, where the linear regression with a larger slope at higher temperatures indicates greater reactivity. As discussed in detail further below, the large difference in k_{obs} between these two

260 temperature regimes coincides with the canola oil substrates being in a liquid and solid phase state, respectively. For the cases of NO$_3$ and OH (Figs. 6b and 6c), the gradual change of k_{obs} coincides with a phase transition for both substrates from a highly viscous liquid to a semi-solid and solid (glassy) phase.

The change in concentration of oxidant X along the flow tube due to reactive uptake can be expressed using the effective uptake coefficient

265 $\gamma_{\mathrm{eff,X}} = \frac{D_{\mathrm{tube}}}{\omega_{\mathrm{X}}} \times \left[ln \left(\frac{[\mathrm{X}]_{\mathrm{g,o}}}{[\mathrm{X}]_{\mathrm{g}}} \right) / t \right] = \frac{D_{\mathrm{tube}}}{\omega_{\mathrm{X}}} \times k_{\mathrm{obs}}$. (3)

Following the Knopf-Pöschl-Shiraiwa (KPS) method (Knopf et al., 2015), actual γ can be derived as:

$\gamma = \frac{\gamma_{\mathrm{eff,X}}}{1 - \gamma_{\mathrm{eff,X}} \frac{3}{2 N_{\mathrm{shw}}^{\mathrm{eff}} K n_{\mathrm{X}}}}$, (4)

where D_{tube} is the diameter of the coated-wall tube and ω_{X} (X = O$_3$, NO$_3$ or OH radical) is the mean molecular velocity of the respective gas-phase oxidant. $N_{\mathrm{Shw}}^{\mathrm{eff}}$ is the effective Sherwood number which represents an effective dimensionless mass-

270 transfer coefficient to account for changes in the radial concentration profile of the entry region (Knopf et al., 2015;Davis, 2008), and Kn_{X} is the Knudsen number that characterizes the flow regime (Wutz, 1989;Fuchs and Sutugin, 1971). The Sherwood number departs from $N_{\mathrm{Shw}}^{\mathrm{eff}}$=3.66 under conditions of fast flows and short tubes. The KPS method is advantageous over the correction approach by Brown (1978) since it accounts for entrance effects that can result in the overestimation of reactive uptake coefficients as outlined by Davis (2008) and discussed in more detail in the Appendix. The Cooney-Kim-Davis

275 (CKD) method (Cooney et al. 1974) also accounts for the flow entrance effects as discussed in Murphy et al. (1987). This is crucial for fast uptakes involving the OH radical, however, less so for the uptakes involving O$_3$ and NO$_3$ radicals. The uncertainty in derived γ values represents the greater value of either a 20% uncertainty in the diffusion coefficient or variation in measurements expressed as ±1σ.

The gas-phase diffusion coefficient of O$_3$ in He ($D_{\mathrm{O_3-He}}$) is taken as 394 Torr cm^2 s^{-1} at 298 K (Moise and Rudich, 2000).

280 Diffusion coefficients of NO$_3$ in He and O$_2$ are taken as 345 and 80 Torr cm^2 s^{-1} at 273 K, respectively (Rudich et al., 1996). The method introduced by Fuller et al. (1966) was utilized for O$_3$ and NO$_3$ to derive the diffusion coefficients at other temperatures. The diffusion coefficients of OH in He and O$_2$ gas ($D_{\mathrm{OH-He}}$ and $D_{\mathrm{OH-O_2}}$) for different temperatures are theoretically calculated based on a method reported by Mason and Monchick (1962). A reference value of $D_{\mathrm{OH-He}}$ measured at room temperature is 662 ± 33 Torr cm^2 s^{-1} (Ivanov et al., 2007;Liu et al., 2009). To calculate the diffusion coefficient of an

285 oxidant (D_{X}) in a mixture of He and O$_2$, we applied the following equation with P_{He} and $P_{\mathrm{O_2}}$ representing pressures derived from experimental flow rates and pressure measurements (Hanson and Ravishankara, 1991)

$$D_X = \frac{P_{He}}{D_{X-He}} + \frac{P_{O_2}}{D_{X-O_2}} \; . \tag{5}$$

The pressure in the flow reactor is maintained at less than 2.5 hPa to avoid transport limitations by diffusion of OH radicals that undergo fast reactive uptake kinetics. Diffusion limitation can be estimated by using the additivity formula for kinetic

290   resistances as (Gershenzon et al., 1995)

$$\frac{1}{k_{obs}} = \frac{1}{k_k} + \frac{1}{k_d} \tag{6}$$

$$k_k = \frac{\omega_X \times \gamma}{R \times (2-\gamma)} \tag{7}$$

$$k_d = 3.66 \frac{D_X}{R^2} \quad , \tag{8}$$

where k_{obs} (s^{-1}) is the observed wall loss rate of heterogeneous uptake, and k_k and k_d represent its kinetic and diffusion limits,

295   respectively. R is the radius of the flow tube. Gershenzon et al. (1995) proposed that k_k/k_d should be < 3~5 to obtain an accurate γ value. Some of the highest temperature OH uptake experiments involving liquid canola oil were conducted under diffusion limitation with $k_k/k_d \cong 15\text{\textasciitilde}30$. However, for all the remaining experiments $k_k/k_d < 5$ and, thus, are not diffusion limited.

As outlined in Supplemental Text S4, for semi-solid and solid substrate films, the fraction of the unoxidized reaction sites

300   is always larger than 90% due to short reaction time and low concentrations of gas oxidants (Bertram et al., 2001), implying no significant surface saturation effect on γ. In other words, during the typical duration of a reactive uptake experiment, the oxidant exposure does not lead to complete oxidation of the substrate surface.

3.3 Temperature modulated reactive O$_3$ uptake

Figure 7 shows γ of O$_3$ reacting with canola oil as a function of temperature. The reactive uptake is determined under dry

305   conditions in the presence of O$_2$. Both Brown and KPS methods were used to derive γ (Brown, 1978;Knopf et al., 2015). Both methods yield the same results due to the slow uptake kinetics as further discussed in the Appendix. Around 90% of canola oil is made up of oleic acid, linoleic acid and α-linolenic acid (Ghazani and Marangoni, 2013), and it solidifies readily around its melting point (de Gouw and Lovejoy, 1998). γ decreases sharply by a factor of ~18 from $(5.65 \pm 0.89) \times 10^{-4}$ to $(3.23 \pm 0.74) \times 10^{-5}$ as the temperature decreases from 267 K to 258 K, a temperature range in which the canola oil experiences a phase

310   transition from liquid to solid (Fasina et al., 2008). In this temperature regime, the bulk diffusion coefficients of both ozone and canola oil are expected to decrease by several orders of magnitude due to the transition from a viscous liquid to a solid (Koop et al., 2011). Our O$_3$ reactive uptake coefficients agree with previous literature data by de Gouw et al. (1998) and extend those to lower temperatures. A study by Berkemeier et al. (2016) showed that the uptake of O$_3$ by shikimic acid is ~5×10^{-6} at low RH conditions and increases by a factor of ~16 at higher RH due to a decrease in viscosity as a result of a RH-induced

315   phase transition, similar to our observations. Our results are consistent with previous studies (Shiraiwa et al., 2009;Shiraiwa et al., 2010;Steimer et al., 2015), which showed that the O$_3$ uptake is slower and restricted to near the particle surface if the organic is in a solid phase, while the uptake is dominated by bulk reaction if the organic is in a liquid phase.

In the low temperature regime, from 213 K to 258 K, γ only increases by about a factor of 1.7 (Fig. 6). If we consider the gas-phase reaction kinetics of O_3 with an unsaturated bond having an activation energy of 15 kJ mol^{-1} (Atkinson et al., 2006),

320   an increase of the reaction rate by a factor of 4.4 would be expected over a temperature of 45 K. This less than expected temperature dependency of γ may be due to the combined temperature effects on both the underlying reaction kinetics and the desorption lifetime (Pöschl et al., 2007). As the temperature decreases and reactivity decreases, the desorption lifetime increases, potentially resulting in a compensating effect on the overall uptake kinetics. In the temperature regime above the phase transition, between 267 K and 293 K, γ is significantly larger than when the canola oil substrate is solid, likely due to

325   greater reaction rates and greater O_3 and condensed-phase diffusion coefficients.

3.4 Temperature modulated reactive NO₃ uptake

The uptake coefficient of NO_3 by levoglucosan (LEV) decreases from $(4.2\pm0.6) \times 10^{-4}$ to $(2.8 \pm 0.3) \times 10^{-4}$ as the temperature decreases from 293 K to 213 K, thus, displaying only a slight change in γ within the experimental temperature range (Fig. 8a). Based on our poke-flow experiment, LEV substrates maintained a semi-solid or solid phase state for all examined temperatures.

330   The slight increase of γ with temperature may due to the slight change in substrate viscosity (see Fig. 4), the counteracting effect of the temperature dependence of the reaction rate (Atkinson et al., 2006) and the desorption lifetime (Pöschl et al. 2007). Note, the γ of **NO₃** by LEV in this experiment is smaller than the value of $(1.3 \pm 0.9) \times 10^{-3}$ determined in our previous study at 298 K, although the data agree within uncertainties (Knopf et al., 2011). A possible explanation for the lower γ value in this study is that the substrates have undergone longer drying to remove residual water. Presence of water would render the film

335   less viscous thereby increasing reactivity.

For the mixture of LEV/XYL (Fig. 8b), γ at 293 K is 8.5×10^{-4}, about a factor of 2 larger than for pure LEV (see Table 2). As the temperature decreases, γ reaches a value of 3.1×10^{-4} at 213 K, similar to the γ value derived for solid LEV (Fig. 8a). The observed change in uptake kinetics is attributed to the phase change of the film substrate. Our poke-flow experiment yielded $T_g = 238$ K for the applied LEV/XYL film. The largest change of γ is observed around the expected T_g (Fig. 8b).

340   Therefore, the significant change in NO_3 uptake reactivity in the investigated temperature range can be attributed to the transition of a liquid to a highly viscous or solid substrate film. As such, the underlying reaction mechanism changes, i.e., at higher temperatures, the kinetic uptake is likely governed by surface and bulk reactions and at lower temperatures only surface reaction dominates. As shown in Shiraiwa et al. (2012), for highly viscous/solid LEV films, the transport of bulk LEV towards the interface is strongly limited, slowing the reactive uptake kinetics. At higher temperatures, with decreasing viscosity of

345   LEV, the diffusivity of LEV and NO_3 increases, likely facilitating transport and thus reaction.

Gross et al. (2009) reported that γ of NO_3 by liquid glycerol (GLY) is $(14\pm3) \times 10^{-4}$ at 293 K and decreases to 8.3×10^{-4} at 268 K, representing a decrease of 41% in γ over 25 K. The T_g of glycerol is 193 K, and the viscosity decreases from 20 Pa s at 268 K to 1.32 Pa s at 293 K (Schröter and Donth, 2000). For the same temperature difference of 25 K, γ for the viscous liquid LEV/XYL substrate decreases by about 24%. The reason for this difference may lie in the higher viscosity of the LEV/XYL substrate within this temperature range. The viscosity of LEV/XYL film is around 10^1 to 10^2 Pa s based on our poke-flow

experiments and viscosity prediction as outlined in section 3.1. Therefore, the lower sensitivity of γ on temperature may be due to the generally higher viscosity compared to a glycerol substrate. Moise et al. (2002) studied the uptake of NO₃ by a saturated alcohol, 1-octanol, in the liquid and solid-phase. They derived γ = 7.1×10⁻³ at 258 K for the liquid phase of 1-octanol and 4.1×10⁻³ at 248 K for the solid phase as shown in Table 2. The change in γ is a factor 1.73 over 10 K, mainly because of

355 the rapid phase transition of 1-octanol. In our LEV/XYL uptake experiment, γ changes by a factor 2.74 over a temperature range of 80 K, however, γ measured here is about one order of magnitude lower. We suggest that the different sensitivity in γ over these different temperature ranges is due to the continuous amorphous phase transition of the LEV/XYL mixture compared to the abrupt phase transition of 1-octanol.

At low temperatures, γ for NO₃ uptake by LEV and LEV/XYL films are similar within our experimental uncertainties, as

360 shown in Table 2. This is in contrast to expectations derived from the gas-phase structure activity relationships (SARs) (Atkinson, 1987;Kerdouci et al., 2014), which predict that the reaction NO₃ + LEV occurs 6.7 times faster than the reaction of NO₃ + XYL. Also, γ of solid LEV and LEV/XYL is similar to NO₃ uptake by solid alkane substrates and monolayers (Knopf et al., 2011;Gross and Bertram, 2009;Moise et al., 2002). However, an alcohol is expected to be more reactive with NO₃ compared to an alkane, as the α-hydrogen atom at the OH group is more labile and thus facilitates the hydrogen abstraction.

365 These measurements indicate that the presence of labile α-hydrogen atoms in solid substrate films do not significantly yield higher γ. A possible explanation may be that the number density of labile α-hydrogen atoms at the interface is not sufficiently different between LEV, the LEV/XYL mixture and alkane substrates films. Furthermore, considering that NO₃ concentrations are too low to saturate the substrate surface, the probability of collisions with the most reactive hydrogen may also be low. This may result in similar γ within our uncertainties, for both substrates. In conclusion, our study demonstrates a strong positive

370 correlation between temperature, substrate phase state, and NO₃ uptake reactivity for saturated alcohols.

3.5 Temperature modulated reactive OH uptake

Figure 9a shows γ of OH reacting with GLU as a function of temperature indicating no significant change in reactivity over the examined temperature range. As the temperature increases from 250 K on, γ appears to slightly decrease from 0.11±0.03 to 0.09 ±0.03, although this change is within experimental uncertainties. GLU substrates maintain a solid or highly viscous

375 phase state for all examined temperatures. The gas-phase structure activity relationship (SAR) predicts that the gas-phase reaction rate of OH radicals with GLU ($k_{\text{Glu}}^{\text{g}}$) decreases by a factor of 2.5 from 213 K to 298 K (Atkinson, 1987;Kwok and Atkinson, 1995). We also observe a decrease in reactivity (Fig. 9a), however, not as strong as during gas-phase reactions. This implies that other factors may also play a role in the observed heterogeneous reactivity. Since different chemical bonds have different reactivity and temperature dependence (Kwok and Atkinson, 1995), the reaction probability of OH radicals can be

380 affected by the molecular orientation at the surface. SAR suggests that tertiary C-H bonds contribute to this negative temperature dependency of the reactivity. Hence, if more C-OH bonds are exposed to the surface compared to tertiary C-H bonds, this negative temperature dependency of reactivity weakens. A similar steric argument was given by Nah et al. (2014), who suggested that the increased surface density of C=C double bonds due to the formation of oleic acid dimers possibly leads

to a faster surface reaction involving OH radicals. Also, the remaining amount of water in these substrates may impact the
385   surface structure and the viscosity of the near-surface region, thereby potentially counteracting the decreasing reaction rate
with increasing temperature predicted by SAR method.

For the GLU/HEX mixture (Fig. 9b), γ at 303 K is 0.13±0.03, ~1.5 times larger than that at 233 K. The larger γ at higher
temperature can be attributed to the viscosity change of the substrate film with increasing temperature. T_g is estimated as (248
± 3) K by our poke-flow experiment. Judging by the morphology and the flow characteristics of the organic film, it experiences
390   a glass phase transition within the investigated temperature range. The major change in γ matches the expected phase change
of the GLU/HEX mixture. γ by GLU/HEX at low temperatures, i.e., between 213 K and 233 K, are lower than γ by GLU, and
this is likely related to the lower reaction rate of HEX with OH radicals. For example, SAR predicts the reaction rate for HEX
+ OH to be 2.6 times slower than that for GLU + OH at 213 K.

Figure 9c shows that γ of CA increases by a factor of 5 within the experimental temperature range, from 0.13 ± 0.08 at
395   213 K to 0.66 ± 0.24 at 293 K. This increase of γ is particularly significant above the melting point of canola oil, $T_m = 258$ K
(Fasina et al., 2008). Therefore, we attribute this large change in γ to the phase and viscosity change of the canola oil. γ
increases by a factor of ~2.4 between 273 K and 293 K, where the viscosity of canola oil changes from 0.185 to 0.079 Pa s
(Fasina et al., 2006). We observed that as the canola oil is in a solid or viscous liquid (grease) state at temperatures between
213 and 253 K, γ is less sensitive to temperature changes compared to when the canola oil is in a liquid phase. γ by CA is
400   larger than γ by GLU at low temperatures although both are in solid phase, thus implying that OH reacts faster with C=C bonds
than with C-H bonds and OH groups present on solid surfaces. Waring et al. (2011) measured the reactive loss of gas-phase
OH radicals on squalene surfaces at room temperature, reporting $\gamma = 0.39 ± 0.07$. These measurements suggest that γ by CA
can be larger than γ by squalene although squalene has more double bonds compared to canola oil and both organics have
similar viscosity (e.g., μ_{Sqe} is 0.012 Pa s at 298 K, Comunas et al., 2013). Different accessibility of C=C bonds on the substrate
405   surfaces could be one reason for different γ values. X-ray diffraction studies on liquid oleic acid showed that the unsaturated
acid molecules exist primarily as dimers through hydrogen bonding of the carbonyl oxygen and the acidic hydrogen (Iwahashi
and Kasahara, 2011;Iwahashi et al., 2000), and this possibly leads to more C=C double bonds at the substrate surface (Hearn
et al., 2005). However, whether or not this phenomenon can compensate for the more numerous C=C double bonds present in
squalene molecules is uncertain. Lastly, gas-phase reaction kinetics suggest that unsaturated oxygenated organics (e.g., acids,
410   alcohols, ketones) are more reactive toward OH radicals than their alkene equivalents due to the formation of a hydrogen
bonded complex that facilities the formation of stable reaction products via interactions between the OH radical and the
oxygenated functional group of the molecule (Mellouki et al., 2003;Orlando et al., 2001).

4 Atmospheric implications

Temperature varies greatly in the troposphere, both in the latitudinal and altitudinal directions. The zonal average surface
415   temperature changes approximately 0.86 K per latitude degree in the northern hemisphere (Gates et al., 1999), and the vertical

temperature gradient is typically defined by the lapse rate of ~10 K km^{-1} for dry air and ~7 K km^{-1} for wet air (Wallace and Hobbs, 2006). Globally, the temperature will greatly influence the phase state and the heterogeneous oxidation of OA particles, especially for SOA particles that can exist a liquid phase state in the warmer planetary boundary layer but can be mostly solid in the colder middle and upper troposphere (Shiraiwa et al., 2017a).

420   The determined γ values can be used to estimate the oxidation lifetime for a solid organic surface with the following equation (Moise and Rudich, 2001):

$$\tau = \frac{4N_{\text{tot}}}{\gamma \omega_X [X]_g} \quad , \tag{9}$$

where τ is the lifetime of one monolayer of coverage, i.e., how long it takes for 63% surface molecules to be oxidized. N_{tot} represents the concentration of reaction sites on the organic substrate surface. Here, we apply this idealized approach to assess

425   the degree of surface oxidation of OA particles in a solid or highly viscous phase state and when the oxidation reactions are confined to the surface. However, given that the surface-active organics are ubiquitous in tropospheric aerosols and organic films can exist on aerosol surfaces with potentially significant effects on atmospheric chemistry and climate, e.g., heterogeneous reactions, particle hygroscopicity, optical properties, and cloud forming activity (Jimenez et al., 2009;Kroll et al., 2015;Katrib et al., 2005b;Knopf et al., 2018;Slade et al., 2017;Robinson et al., 2007;Shiraiwa et al., 2017a;Cosman and

430   Bertram, 2008;McNeill et al., 2006;Knopf et al., 2007;Knopf and Forrester, 2011;Moise et al., 2015), this approach can further our understanding of the chemical evolution of atmospheric OA. We assume $N_{\text{tot}} = 10^{15}$ cm^{-2} (Bertram et al., 2001). The concentration of gas oxidants O$_3$, NO$_3$, and OH are based on ambient conditions as 1×10^{12}, 1.25×10^9 and 1×10^6 molecules cm^{-3}, respectively (Finlayson-Pitts and Pitts Jr, 1999). Figure 10 shows the effect of temperature on the surface species' lifetime for the different examined heterogeneous oxidation reactions. Oxidation of CA by O$_3$ proceeds within minutes to hours for

435   typical tropospheric temperatures. Thus, degradation of unsaturated fatty acids is expected to proceed efficiently, even at colder temperatures. Despite the OH radical being the most effective oxidizer, Fig. 10 suggests that for middle and upper tropospheric conditions, oxidation of the particle surface by OH can take 1 to 2 weeks, emphasizing the slow physicochemical changes of the particle properties during transport at high altitudes. However, closer to the surface, degradation can proceed almost an order of magnitude faster. Degradation of the particle surface by NO$_3$ may proceed by about a factor 2 slower at the coldest

440   tropospheric temperatures compared to boundary layer conditions. Clearly, these datasets indicate that the topmost organic layers for most of the investigated OA surrogates can be oxidized within 1 week for lower and middle tropospheric conditions. However, as soon as OA particles reach higher altitudes and lower temperatures by, e.g., pyro-convection (Andreae et al., 2004;Jost et al., 2004;Fromm and Servranckx, 2003), their atmospheric lifetime increases significantly. For example, aerosol particles originating from extreme wildfires like an Australia bushfire can circumnavigate the globe in weeks and can even

445   reach the stratosphere existing for weeks or months (Ribeiro et al., 2020).

For OA particles, the lifetime (τ_p) and particle degraded fraction (DF) can be estimated by the equations below (George et al., 2007):

$$\tau_p = \frac{4}{3} \frac{\rho R N_a}{\gamma \omega_X [X]_g M} \tag{10}$$

and

450 $$DF = 1 - \exp\left(-\frac{t}{\tau_\mathrm{p}}\right),\tag{11}$$

where R is the radius of the particle, chosen here as 100 nm, N_a is Avagadro's number, M is the molecular weight of the condensed-phase species, and t is time. We derive DF as a function of temperature and oxidant exposure time for oxidant concentrations given above. However, we note that this DF estimate is a simplified approach, since we assume that measured oxidation kinetics proceed throughout the entire particle with the same rate. This ignores the slow gas diffusion in the

455 condensed phase and the hindered internal mixing of organic species, particularly when the OA particle is in a solid or highly viscous phase state. As such, the DF values at lower temperatures likely represent upper limits. In other words, degradation in ambient particles is expected to be less. Keeping this limitation in mind, Fig. 11 displays the estimated DF for the examined oxidant-surrogate systems. As expected, for the lowest temperatures, the DF values are lowest, implying longest lifetimes. The stronger the particle viscosity change with temperature, the greater is the change in DF, e.g., viscosity of CA decreases from

460 10^{12} to 10^{-2} Pa s over 213 to 293 K. This yields the largest change in DF over this temperature range compared to the other investigated systems (considering the same exposure time period). Figures 11(c) and (d) display a small DF within one month for LEV/XYL and GLU/HEX mixtures in the upper troposphere. This is consistent with previous aircraft observations reporting a large amount of biomass burning aerosol particles in aged plumes at higher altitudes of the troposphere (Cubison et al., 2011). This also supports the hypothesis that aerosol particles originating from large wildfires (e.g., Australian bushfires)

465 can be transported into the northern hemisphere from the stratosphere within a time period of one year (Deshler, 2008; Peterson et al., 2018).

5 Conclusions

In this study, we measured γ for several systems of oxidant and organic aerosol surrogate combinations including O_3 and OH + CA, NO_3 + LEV and LEV/XYL, OH + GLU and GLU/HEX, under dry conditions and for temperatures ranging from 213

470 K to 313 K. For the case of OH, this is the first low temperature reactive uptake study of which the authors are aware. The phase states of the organic substrate films were examined using the poke-flow technique allowing for an estimation of T_g and substrate flow characteristics to constrain the magnitude of the substrate viscosity at different temperatures using the VTF equation.

The strongest changes in heterogeneous reactivity observed for the examined oxidant-substrate systems correlates with

475 the largest change in organic substrate viscosity with temperature associated with a solid-to-liquid phase transition. The largest reactivity occurs between O_3 and CA exhibiting a change by a factor of 34, due to the phase transition of CA. In general, we attribute the faster heterogeneous kinetics in the semi-solid and liquid phase state to surface and bulk reactions, the latter enabled by increased diffusion coefficients of gas and condensed species resulting from lower viscosity. LEV and GLU substrates display a semi-solid and solid phase state over the entire probed temperature range, with estimated viscosities larger

480   than 10^4 Pa s. As a result, the overall reactivity is lower compared to liquid substrate films and does not change significantly with temperature. In this case, surface reactions likely dominate and replenishment of unoxidized molecules to the surface is hindered. Application of organic substrate mixtures to control T_g to induce a solid-to-liquid phase transition as temperature increases, is accompanied with an increase in reactivity.

Our results are consistent with previous studies reporting the significance of particle phase state for the reactive uptake
485   kinetics (Arangio et al., 2015;Knopf et al., 2005;Kolesar et al., 2014;Slade and Knopf, 2014;Davies and Wilson, 2015;Shiraiwa et al., 2012). To resolve the molecular processes of the measured heterogeneous kinetics, detailed modelling studies (Pöschl et al., 2007;Shiraiwa et al., 2010;Arangio et al., 2015;Houle et al., 2015;Houle et al., 2018;Pöschl and Shiraiwa, 2015) extended to lower temperatures are needed. A crucial aspect of this study is the interplay between the temperature dependence of the reaction kinetics and the desorption lifetime. At lower temperatures when an organic substrate in the solid state, over a wide
490   temperature range the reactivity does not change significantly. Desorption lifetime will likely increase significantly with decreasing temperature with subsequent effects on the reaction kinetics. Small changes in viscosity with temperature may also play a role in the overall heterogeneous kinetics when the substrate is in a semi-solid phase state. However, to what extent the particle viscosity will influence the diffusion and reaction kinetics is still not resolved. The comprehensive data set presented here will allow application of a more detailed kinetic multi-layer model to constrain the temperature dependency of reaction
495   and transport parameters.

Our study demonstrates unambiguously that the chemical reactivity of organic matter towards atmospheric oxidants can vary significantly in response to ambient temperature, which, in turn, modulates the organic phase state. As a result, we can expect OA particles during transport in the free troposphere to have significantly longer lifetimes with respect to chemical degradation. This is important information for our understanding of the chemical evolution of OA particles and their impact
500   on source apportionment, air quality, and climate.

6 Appendix: The impact of gas flow entrance effects and velocity profiles on the reactive uptake kinetics

The KPS method (Knopf et al., 2015), similar to the Cooney-Kim-Davis (CKD) method applied by Murphy and Fahey (1987) , accounts for gas flow entrance effects into the flow reactor, i.e., the establishment of concentration profiles, that impact the derivation of the reactive uptake coefficient as pointed out by Davis (2008). When considering the establishment of gas
505   concentration profiles for correction of observed pseudo-first order wall loss rates, slower uptake reaction kinetics (e.g., the uptake of O_3), typically represent conditions of either having a slow gas flow or long flow tube, and thus the $N_{shw}^{eff} \approx 3.66$ as shown in Fig. A1 (Davis, 2008). In this case, the different approaches (Brown, CKD, and KPS) to correct observed wall loss rate for transport limitations by diffusion yield the same γ values as illustrated in Fig. 7 (CKD approach is not shown but yields same results as KPS). However, reactive OH uptake exerts faster reaction kinetics and thus resembles conditions of a fast gas
510   flow or a short flow tube (Fig. A1) where N_{shw}^{eff} can significantly depart from 3.66 (Knopf et al., 2015;Murphy and Fahey, 1987;Davis, 2008). In this case, γ values derived by the Brown method always yield larger values compared to those derived

by the KPS method as illustrated in Fig. A2 for the uptake of OH by glucose. Hence, for fast uptake kinetics, we recommend using either the KPS or CKD methods to derive accurate uptake kinetics when using a coated-wall flow reactor.

515 The gas flow velocity ratio between mean flow velocities in the flow reactor (u_{mean}^{ann}) and the gas flow exiting the movable injector (u_{mean}^{inj}) also impacts the derivation of γ. If $u_{mean}^{ann} < u_{mean}^{inj}$, reactive uptake experiments are ambiguous, potentially resulting in an underestimation of the uptake kinetics, as pointed out by Davis (2008). This flow condition can lead to a jet-like exit gas flow from the movable injector. Figure A2 displays this effect when $u_{mean}^{ann}/u_{mean}^{inj} < 1$, where the measured γ values can deviate by a factor of 3 from the actual value.

For all experimentally derived γ values, we set $u_{mean}^{ann}/u_{mean}^{inj} > 1.27$ for the flow tube with 1.758 cm inner diameter (ID) 520 and $u_{mean}^{ann}/u_{mean}^{inj} > 1.33$ for the flow tube with an ID of 1.2 cm, based on the theoretical calculation below. The velocity profile and volume flow rate Q of a Poiseuille flow in the annular section can be described by the equations (Rosenhead, 1988)

$$u(r) = \frac{G}{4\mu}\left[(R_1^2 - r^2) + (R_2^2 - R_1^2)\frac{\ln(r/R_1)}{\ln(R_2/R_1)}\right] \tag{A1}$$

and

$$Q = \int_{R_1}^{R_2} 2\pi r u(r)dr = \frac{G\pi}{8\mu}\left[R_2^4 - R_1^4 - \frac{(R_2^2 - R_1^2)^2}{\ln(R_2/R_1)}\right] , \tag{A2}$$

525 where $u(r)$ is the flow velocity profile as a function of the radius r. G is a constant pressure gradient, μ is the dynamic viscosity, R_1 is the inner cylinder radius, R_2 is the outer cylinder radius, and r is a radius value between R_1 and R_2. If R_1, R_2 and constant parameters (G and μ) are known, the maximum flow velocity u_{max} is obtained by setting $du(r)/dr = 0$, and the mean flow velocity in the annular section u_{mean} is derived from Q/A_{ann}, where A_{ann} is the cross-sectional area of the annular section.

Using the flow tube with a diameter of 1.758 cm as an example, and setting $R_1 = 0.325$ cm and $R_2 = 0.879$ cm, the ratio of 530 maximum flow velocity over the average flow velocity in the annular section is $u_{max}^{ann}/u_{mean}^{annul} = 1.575$. The ratio of the mean flow velocity over the maximum velocity in a tubular injector is $u_{max}^{inj}/u_{mean}^{inj} = 2$ as the injector flow is laminar (Rogers, 1992). Therefore, even when adjusting the gas flows in the injector and flow reactor to yield the same mean flow velocities, the difference in the maximum flow velocities can still differ significantly. In this case, the difference can be up to 27%, potentially resulting in a jet-like gas flow profile. For this reason, we set $u_{mean}^{ann}/u_{mean}^{inj} > 1.27$ to avoid this effect. In the case of using a 535 flow tube with a diameter of 1.2 cm, $u_{mean}^{ann}/u_{mean}^{inj} > 1.33$.

Data availability

Data and code generated from this study are available from the corresponding author upon request.

Author contributions

JL conducted O₃, NO₃, and OH uptake experiments. SF performed N_2O_5 synthesis and conducted NO_3 uptake experiments. JL
540   conducted the poke-flow experiments. JL performed all analysis of data. SF conducted analysis of NO_3 uptake data and
contributed to the writing of the manuscript. JL led the writing of the manuscript. DK oversaw the project, envisioned analysis,
and contributed to the writing of the manuscript.

Competing interest

The authors declare no conflict of interest.

545   **Acknowledgements**

Support from the National Science Foundation grant AGS-1446286 is acknowledged. Partial support from the U.S. Department
of Energy, Office of Science (BER), Atmospheric System Research (DE-SC0016370), is acknowledged.

References

Abbatt, J. P. D., Leaitch, W. R., Aliabadi, A. A., Bertram, A. K., Blanchet, J. P., Boivin-Rioux, A., Bozem, H., Burkart, J., Chang, R. Y. W.,
550   Charette, J., Chaubey, J. P., Christensen, R. J., Cirisan, A., Collins, D. B., Croft, B., Dionne, J., Evans, G. J., Fletcher, C. G., Gali, M.,
Ghahremaninezhad, R., Girard, E., Gong, W. M., Gosselin, M., Gourdal, M., Hanna, S. J., Hayashida, H., Herber, A. B., Hesaraki, S., Hoor,
P., Huang, L., Hussherr, R., Irish, V. E., Keita, S. A., Kodros, J. K., Kollner, F., Kolonjari, F., Kunkel, D., Ladino, L. A., Law, K., Levasseur,
M., Libois, Q., Liggio, J., Lizotte, M., Macdonald, K. M., Mahmood, R., Martin, R. V., Mason, R. H., Miller, L. A., Moravek, A., Mortenson,
E., Mungall, E. L., Murphy, J. G., Namazi, M., Norman, A. L., O'Neill, N. T., Pierce, J. R., Russell, L. M., Schneider, J., Schulz, H., Sharma,
555   S., Si, M., Staebler, R. M., Steiner, N. S., Thomas, J. L., von Salzen, K., Wentzell, J. J. B., Willis, M. D., Wentworth, G. R., Xu, J. W., and
Yakobi-Hancock, J. D.: Overview paper: New insights into aerosol and climate in the Arctic, Atmos. Chem. Phys., 19, 2527-2560,
http://doi.org/10.5194/acp-19-2527-2019, 2019.
Abramson, E., Imre, D., Beranek, J., Wilson, J., and Zelenyuk, A.: Experimental determination of chemical diffusion within secondary
organic aerosol particles, Phys. Chem. Chem. Phys., 15, 2983-2991, http://doi.org/10.1039/c2cp44013j, 2013.
560   Andreae, M. O., Rosenfeld, D., Artaxo, P., Costa, A. A., Frank, G. P., Longo, K. M., and Silva-Dias, M. A.: Smoking rain clouds over the
Amazon, Science, 303, 1337-1342, http://doi.org/10.1126/science.1092779, 2004.
Angell, C. A.: Relaxation in liquids, polymers and plastic crystals - strong fragile patterns and problems, J. Non-Cryst. Solids, 131, 13-31,
http://doi.org/10.1016/0022-3093(91)90266-9, 1991.
Angell, C. A.: Formation of glasses from liquids and biopolymers, Science, 267, 1924-1935, http://doi.org/10.1126/science.267.5206.1924,
565   1995.
Angell, C. A.: Liquid fragility and the glass transition in water and aqueous solutions, Chem. Rev., 102, 2627-2650,
http://doi.org/10.1021/cr000689q, 2002.
Arangio, A. M., Slade, J. H., Berkemeier, T., Poschl, U., Knopf, D. A., and Shiraiwa, M.: Multiphase chemical kinetics of OH radical uptake
by molecular organic markers of biomass burning aerosols: humidity and temperature dependence, surface reaction, and bulk diffusion, J.
570   Phys. Chem. A, 119, 4533-4544, http://doi.org/10.1021/jp510489z, 2015.
Atkinson, R.: A structure-activity relationship for the estimation of rate constants for the gas-phase reactions of OH radicals with organic
compounds, Int. J. Chem. Kinet., 19, 799-828, http://doi.org/10.1002/kin.550190903, 1987.
Atkinson, R., Baulch, D. L., Cox, R. A., Crowley, J. N., Hampson, R. F., Hynes, R. G., Jenkin, M. E., Rossi, M. J., and Troe, J.: Evaluated
kinetic and photochemical data for atmospheric chemistry: Volume I - gas phase reactions of Ox, HOx, NOx and SOx species, Atmos. Chem.
575   Phys., 4, 1461-1738, http://doi.org/10.5194/acp-4-1461-2004, 2004.

Atkinson, R., Baulch, D. L., Cox, R. A., Crowley, J. N., Hampson, R. F., Hynes, R. G., Jenkin, M. E., Rossi, M. J., and Troe, J.: Evaluated kinetic and photochemical data for atmospheric chemistry: Volume II - gas phase reactions of organic species, Atmos. Chem. Phys., 6, 3625-4055, http://doi.org/10.5194/acp-6-3625-2006, 2006.

Baetzold, R., and Somorjai, G. A.: Preexponential factors in surface reactions, J. Catal., 45, 94-105, http://doi.org/10.1016/0021-9517(76)90059-2, 1976.

Bai, J., Sun, X., Zhang, C., Xu, Y., and Qi, C.: The OH-initiated atmospheric reaction mechanism and kinetics for levoglucosan emitted in biomass burning, Chemosphere, 93, 2004-2010, http://doi.org/10.1016/j.chemosphere.2013.07.021, 2013.

Berkemeier, T., Steimer, S. S., Krieger, U. K., Peter, T., Poschl, U., Ammann, M., and Shiraiwa, M.: Ozone uptake on glassy, semi-solid and liquid organic matter and the role of reactive oxygen intermediates in atmospheric aerosol chemistry, Phys. Chem. Chem. Phys., 18, 12662-12674, http://doi.org/10.1039/c6cp00634e, 2016.

Bertram, A. K., Ivanov, A. V., Hunter, M., Molina, L. T., and Molina, M. J.: The reaction probability of OH on organic surfaces of tropospheric interest, J. Phys. Chem. A, 105, 9415-9421, http://doi.org/10.1021/jp0114034, 2001.

Borde, B., Bizot, H., Vigier, G., and Buleon, A.: Calorimetric analysis of the structural relaxation in partially hydrated amorphous polysaccharides. I. Glass transition and fragility, Carbohyd. Polym., 48, 83-96, http://doi.org/10.1016/s0144-8617(01)00217-x, 2002.

Brown, R.: Tubular flow reactors with first-order kinetics, J. Res. Natl. Bur. Stand, 83, 1-8, 1978.

Brown, S. S., Ryerson, T. B., Wollny, A. G., Brock, C. A., Peltier, R., Sullivan, A. P., Weber, R. J., Dube, W. P., Trainer, M., Meagher, J. F., Fehsenfeld, F. C., and Ravishankara, A. R.: Variability in nocturnal nitrogen oxide processing and its role in regional air quality, Science, 311, 67-70, http://doi.org/10.1126/science.1120120, 2006.

Chenyakin, Y., Ullmann, D. A., Evoy, E., Renbaum-Wolff, L., Kamal, S., and Bertram, A. K.: Diffusion coefficients of organic molecules in sucrose-water solutions and comparison with Stokes-Einstein predictions, Atmos. Chem. Phys., 17, 2423-2435, http://doi.org/10.5194/acp-17-2423-2017, 2017.

Comunas, M. J. P., Paredes, X., Gacino, F. M., Fernandez, J., Bazile, J. P., Boned, C., Daridon, J. L., Galliero, G., Pauly, J., Harris, K. R., Assael, M. J., and Mylona, S. K.: Reference Correlation of the Viscosity of Squalane from 273 to 373 K at 0.1 MPa, J. Phys. Chem. Ref. Data, 42, http://doi.org/10.1063/1.4812573, 2013.

Cosman, L. M., and Bertram, A. K.: Reactive uptake of N2O5 on aqueous H2SO4 solutions coated with 1-component and 2-component monolayers, J. Phys. Chem. A, 112, 4625-4635, http://doi.org/10.1021/jp8005469, 2008.

Cubison, M. J., Ortega, A. M., Hayes, P. L., Farmer, D. K., Day, D., Lechner, M. J., Brune, W. H., Apel, E., Diskin, G. S., Fisher, J. A., Fuelberg, H. E., Hecobian, A., Knapp, D. J., Mikoviny, T., Riemer, D., Sachse, G. W., Sessions, W., Weber, R. J., Weinheimer, A. J., Wisthaler, A., and Jimenez, J. L.: Effects of aging on organic aerosol from open biomass burning smoke in aircraft and laboratory studies, Atmos. Chem. Phys., 11, 12049-12064, http://doi.org/10.5194/acp-11-12049-2011, 2011.

Davies, J. F., and Wilson, K. R.: Nanoscale interfacial gradients formed by the reactive uptake of OH radicals onto viscous aerosol surfaces, Chem Sci, 6, 7020-7027, http://doi.org/10.1039/c5sc02326b, 2015.

Davies, J. F., and Wilson, K. R.: Raman Spectroscopy of Isotopic Water Diffusion in Ultraviscous, Glassy, and Gel States in Aerosol by Use of Optical Tweezers, Anal. Chem., 88, 2361-2366, http://doi.org/10.1021/acs.analchem.5b04315, 2016.

Davis, E. J.: Interpretation of uptake coefficient data obtained with flow tubes, J. Phys. Chem. A, 112, 1922-1932, http://doi.org/10.1021/jp074939j, 2008.

de Gouw, J. A., and Lovejoy, E. R.: Reactive uptake of ozone by liquid organic compounds, Geophys. Res. Lett., 25, 931-934, http://doi.org/10.1029/98gl00515, 1998.

DeRieux, W.-S. W., Li, Y., Lin, P., Laskin, J., Laskin, A., Bertram, A. K., Nizkorodov, S. A., and Shiraiwa, M.: Predicting the glass transition temperature and viscosity of secondary organic material using molecular composition, Atmos. Chem. Phys., 18, 6331-6351, http://doi.org/10.5194/acp-18-6331-2018, 2018.

Deshler, T.: A review of global stratospheric aerosol: Measurements, importance, life cycle, and local stratospheric aerosol, Atmos. Res., 90, 223-232, http://doi.org/10.1016/j.atmosres.2008.03.016, 2008.

Edebeli, J., Ammann, M., and Bartels-Rausch, T.: Microphysics of the aqueous bulk counters the water activity driven rate acceleration of bromide oxidation by ozone from 289-245 K, Environ Sci Process Impacts, 21, 63-73, http://doi.org/10.1039/c8em00417j, 2019.

Elias, M. E., and Elias, A. M.: Trehalose plus water fragile system: properties and glass transition, J. Mol. Liq., 83, 303-310, http://doi.org/10.1016/s0167-7322(99)00094-x, 1999.

Ervens, B., Turpin, B. J., and Weber, R. J.: Secondary organic aerosol formation in cloud droplets and aqueous particles (aqSOA): a review of laboratory, field and model studies, Atmos. Chem. Phys., 11, 11069-11102, http://doi.org/10.5194/acp-11-11069-2011, 2011.

Fasina, O. O., Hallman, H., Craig-Schmidt, M., and Clements, C.: Predicting temperature-dependence viscosity of vegetable oils from fatty acid composition, J. Am. Oil Chem. Soc., 83, 899-903, http://doi.org/10.1007/s11746-006-5044-8, 2006.

Fasina, O. O., Craig-Schmidt, M., Colley, Z., and Hallman, H.: Predicting melting characteristics of vegetable oils from fatty acid composition, LWT-Food Sci. Technol., 41, 1501-1505, http://doi.org/10.1016/j.lwt.2007.09.012, 2008.

Finlayson-Pitts, B. J., and Pitts Jr, J. N.: Chemistry of the upper and lower atmosphere: theory, experiments, and applications, Academic, San Diego, 969 pp., 1999.

Fromm, M. D., and Servranckx, R.: Transport of forest fire smoke above the tropopause by supercell convection, Geophys. Res. Lett., 30, 1542, http://doi.org/10.1029/2002gl016820, 2003.

Fuchs, N., and Sutugin, A. G.: High-dispersed aerosols, in: Topics in current aerosol research, Pergamon Press, Oxford, 1, http://doi.org/10.1016/B978-0-08-016674-2.50006-6, 1971.

Fuller, E. N., Schettler, P. D., and Giddings, J. C.: New Method for Prediction of Binary Gas-Phase Diffusion Coefficients, Ind. Eng. Chem., 58, 18-27, http://doi.org/10.1021/ie50677a007, 1966.

Gates, W. L., Boyle, J. S., Covey, C., Dease, C. G., Doutriaux, C. M., Drach, R. S., Fiorino, M., Gleckler, P. J., Hnilo, J. J., Marlais, S. M., Phillips, T. J., Potter, G. L., Santer, B. D., Sperber, K. R., Taylor, K. E., and Williams, D. N.: An Overview of the Results of the Atmospheric Model Intercomparison Project (AMIP I), Bull. Am. Meteorol. Soc., 80, 29-55, http://doi.org/10.1175/1520-0477(1999)080<0029:Aootro>2.0.Co;2, 1999.

George, I. J., Vlasenko, A., Slowik, J. G., Broekhuizen, K., and Abbatt, J. P. D.: Heterogeneous oxidation of saturated organic aerosols by hydroxyl radicals: uptake kinetics, condensed-phase products, and particle size change, Atmos. Chem. Phys., 7, 4187-4201, http://doi.org/10.5194/acp-7-4187-2007, 2007.

George, I. J., and Abbatt, J. P.: Heterogeneous oxidation of atmospheric aerosol particles by gas-phase radicals, Nat. Chem., 2, 713-722, http://doi.org/10.1038/nchem.806, 2010.

Gershenzon, Y. M., Grigorieva, V. M., Ivanov, A. V., and Remorov, R. G.: O-3 and OH sensitivity to heterogeneous sinks of HOx and CH3O2 on aerosol particles, Faraday Discuss., 100, 83-100, http://doi.org/10.1039/fd9950000083, 1995.

Ghazani, S. M., and Marangoni, A. G.: Minor Components in Canola Oil and Effects of Refining on These Constituents: A Review, J. Am. Oil Chem. Soc., 90, 923-932, http://doi.org/10.1007/s11746-013-2254-8, 2013.

Gordon, M., and Taylor, J. S.: Ideal copolymers and the second-order transitions of synthetic rubbers. i. non-crystalline copolymers, J. Appl. Chem., 2, 493-500, http://doi.org/10.1002/jctb.5010020901, 2007.

Gross, S., and Bertram, A. K.: Products and kinetics of the reactions of an alkane monolayer and a terminal alkene monolayer with NO3 radicals, J. Geophys. Res-Atmos., 114, http://doi.org/10.1029/2008jd010987, 2009.

Gross, S., Iannone, R., Xiao, S., and Bertram, A. K.: Reactive uptake studies of NO3 and N2O5 on alkenoic acid, alkanoate, and polyalcohol substrates to probe nighttime aerosol chemistry, Phys. Chem. Chem. Phys., 11, 7792-7803, http://doi.org/10.1039/b904741g, 2009.

Hallquist, M., Wenger, J. C., Baltensperger, U., Rudich, Y., Simpson, D., Claeys, M., Dommen, J., Donahue, N. M., George, C., Goldstein, A. H., Hamilton, J. F., Herrmann, H., Hoffmann, T., Iinuma, Y., Jang, M., Jenkin, M. E., Jimenez, J. L., Kiendler-Scharr, A., Maenhaut, W., McFiggans, G., Mentel, T. F., Monod, A., Prévôt, A. S. H., Seinfeld, J. H., Surratt, J. D., Szmigielski, R., and Wildt, J.: The formation, properties and impact of secondary organic aerosol: current and emerging issues, Atmos. Chem. Phys., 9, 5155-5236, http://doi.org/10.5194/acp-9-5155-2009, 2009.

Hanson, D. R., and Ravishankara, A. R.: The reaction probabilities of ClONO2 and N2O5 on polar stratospheric cloud materials, J. Geophys. Res., 96, 5081-5090, http://doi.org/10.1029/90jd02613, 1991.

Hearn, J. D., Lovett, A. J., and Smith, G. D.: Ozonolysis of oleic acid particles: evidence for a surface reaction and secondary reactions involving Criegee intermediates, Phys. Chem. Chem. Phys., 7, 501-511, http://doi.org/10.1039/b414472d, 2005.

Hopke, P. K.: Review of receptor modeling methods for source apportionment, J. Air Waste Manage., 66, 237-259, http://doi.org/10.1080/10962247.2016.1140693, 2016.

Houle, F. A., Hinsberg, W. D., and Wilson, K. R.: Oxidation of a model alkane aerosol by OH radical: the emergent nature of reactive uptake, Phys. Chem. Chem. Phys., 17, 4412-4423, http://doi.org/10.1039/c4cp05093b, 2015.

Houle, F. A., Wiegel, A. A., and Wilson, K. R.: Predicting Aerosol Reactivity Across Scales: from the Laboratory to the Atmosphere, Environmental Science & Technology, 52, 13774-13781, http://doi.org/10.1021/acs.est.8b04688, 2018.

Hu, W. W., Palm, B. B., Day, D. A., Campuzano-Jost, P., Krechmer, J. E., Peng, Z., de Sa, S. S., Martin, S. T., Alexander, M. L., Baumann, K., Hacker, L., Kiendler-Scharr, A., Koss, A. R., de Gouw, J. A., Goldstein, A. H., Seco, R., Sjostedt, S. J., Park, J. H., Guenther, A. B., Kim, S., Canonaco, F., Prevot, A. S. H., Brune, W. H., and Jimenez, J. L.: Volatility and lifetime against OH heterogeneous reaction of ambient isoprene-epoxydiols-derived secondary organic aerosol (IEPOX-SOA), Atmos. Chem. Phys., 16, 11563-11580, http://doi.org/10.5194/acp-16-11563-2016, 2016.

Ivanov, A. V., Trakhtenberg, S., Bertram, A. K., Gershenzon, Y. M., and Molina, M. J.: OH, HO2, and ozone gaseous diffusion coefficients, J. Phys. Chem. A, 111, 1632-1637, http://doi.org/10.1021/jp066558w, 2007.

Iwahashi, M., Kasahara, Y., Matsuzawa, H., Yagi, K., Nomura, K., Terauchi, H., Ozaki, Y., and Suzuki, M.: Self-Diffusion, Dynamical Molecular Conformation, and Liquid Structures of n-Saturated and Unsaturated Fatty Acids, J. Phys. Chem. B, 104, 6186-6194, http://doi.org/10.1021/jp000610l, 2000.

Iwahashi, M., and Kasahara, Y.: Dynamic molecular movements and aggregation structures of lipids in a liquid state, Curr. Opin. Colloid In., 16, 359-366, http://doi.org/10.1016/j.cocis.2011.06.005, 2011.

Jimenez, J. L., Canagaratna, M. R., Donahue, N. M., Prevot, A. S., Zhang, Q., Kroll, J. H., DeCarlo, P. F., Allan, J. D., Coe, H., Ng, N. L., Aiken, A. C., Docherty, K. S., Ulbrich, I. M., Grieshop, A. P., Robinson, A. L., Duplissy, J., Smith, J. D., Wilson, K. R., Lanz, V. A., Hueglin, C., Sun, Y. L., Tian, J., Laaksonen, A., Raatikainen, T., Rautiainen, J., Vaattovaara, P., Ehn, M., Kulmala, M., Tomlinson, J. M., Collins, D. R., Cubison, M. J., Dunlea, E. J., Huffman, J. A., Onasch, T. B., Alfarra, M. R., Williams, P. I., Bower, K., Kondo, Y., Schneider,

J., Drewnick, F., Borrmann, S., Weimer, S., Demerjian, K., Salcedo, D., Cottrell, L., Griffin, R., Takami, A., Miyoshi, T., Hatakeyama, S., Shimono, A., Sun, J. Y., Zhang, Y. M., Dzepina, K., Kimmel, J. R., Sueper, D., Jayne, J. T., Herndon, S. C., Trimborn, A. M., Williams, L. R., Wood, E. C., Middlebrook, A. M., Kolb, C. E., Baltensperger, U., and Worsnop, D. R.: Evolution of organic aerosols in the atmosphere, Science, 326, 1525-1529, http://doi.org/10.1126/science.1180353, 2009.

Jost, H. J., Drdla, K., Stohl, A., Pfister, L., Loewenstein, M., Lopez, J. P., Hudson, P. K., Murphy, D. M., Cziczo, D. J., Fromm, M., Bui, T. P., Dean-Day, J., Gerbig, C., Mahoney, M. J., Richard, E. C., Spichtinger, N., Pittman, J. V., Weinstock, E. M., Wilson, J. C., and Xueref, I.: In-situ observations of mid-latitude forest fire plumes deep in the stratosphere, Geophys. Res. Lett., 31, L11101, http://doi.org/10.1029/2003gl019253, 2004.

Kaiser, J. C., Riemer, N., and Knopf, D. A.: Detailed heterogeneous oxidation of soot surfaces in a particle-resolved aerosol model, Atmos. Chem. Phys., 11, 4505-4520, http://doi.org/10.5194/acp-11-4505-2011, 2011.

Kanakidou, M., Seinfeld, J. H., Pandis, S. N., Barnes, I., Dentener, F. J., Facchini, M. C., Van Dingenen, R., Ervens, B., Nenes, A., Nielsen, C. J., Swietlicki, E., Putaud, J. P., Balkanski, Y., Fuzzi, S., Horth, J., Moortgat, G. K., Winterhalter, R., Myhre, C. E. L., Tsigaridis, K., Vignati, E., Stephanou, E. G., and Wilson, J.: Organic aerosol and global climate modelling: a review, Atmos. Chem. Phys., 5, 1053-1123, http://doi.org/10.5194/acp-5-1053-2005, 2005.

Katrib, Y., Biskos, G., Buseck, P. R., Davidovits, P., Jayne, J. T., Mochida, M., Wise, M. E., Worsnop, D. R., and Martin, S. T.: Ozonolysis of mixed oleic-acid/stearic-acid particles: reaction kinetics and chemical morphology, J. Phys. Chem. A, 109, 10910-10919, http://doi.org/10.1021/jp054714d, 2005a.

Katrib, Y., Martin, S. T., Rudich, Y., Davidovits, P., Jayne, J. T., and Worsnop, D. R.: Density changes of aerosol particles as a result of chemical reaction, Atmos. Chem. Phys., 5, 275-291, http://doi.org/10.5194/acp-5-275-2005, 2005b.

Kerdouci, J., Picquet-Varrault, B., and Doussin, J.-F.: Structure–activity relationship for the gas-phase reactions of NO3 radical with organic compounds: Update and extension to aldehydes, Atmos. Environ., 84, 363-372, http://doi.org/10.1016/j.atmosenv.2013.11.024, 2014.

Kessler, S. H., Smith, J. D., Che, D. L., Worsnop, D. R., Wilson, K. R., and Kroll, J. H.: Chemical sinks of organic aerosol: kinetics and products of the heterogeneous oxidation of erythritol and levoglucosan, Environ. Sci. Technol., 44, 7005-7010, http://doi.org/10.1021/es101465m, 2010.

Kiland, K. J., Maclean, A. M., Kamal, S., and Bertram, A. K.: Diffusion of Organic Molecules as a Function of Temperature in a Sucrose Matrix (a Proxy for Secondary Organic Aerosol), J. Phys. Chem. Lett., 10, 5902-+, http://doi.org/10.1021/acs.jpclett.9b02182, 2019.

Knopf, D. A., Anthony, L. M., and Bertram, A. K.: Reactive uptake of O3 by multicomponent and multiphase mixtures containing oleic acid, J. Phys. Chem. A, 109, 5579-5589, http://doi.org/10.1021/jp0512513, 2005.

Knopf, D. A., Mak, J., Gross, S., and Bertram, A. K.: Does atmospheric processing of saturated hydrocarbon surfaces by NO3 lead to volatilization?, Geophys. Res. Lett., 33, L17816, http://doi.org/10.1029/2006gl026884, 2006.

Knopf, D. A., Cosman, L. M., Mousavi, P., Mokamati, S., and Bertram, A. K.: A novel flow reactor for studying reactions on liquid surfaces coated by organic monolayers: methods, validation, and initial results, J. Phys. Chem. A, 111, 11021-11032, http://doi.org/10.1021/jp075724c, 2007.

Knopf, D. A., and Forrester, S. M.: Freezing of water and aqueous NaCl droplets coated by organic monolayers as a function of surfactant properties and water activity, J. Phys. Chem. A, 115, 5579-5591, http://doi.org/10.1021/jp2014644, 2011.

Knopf, D. A., Forrester, S. M., and Slade, J. H.: Heterogeneous oxidation kinetics of organic biomass burning aerosol surrogates by O3, NO2, N2O5, and NO3, Phys. Chem. Chem. Phys., 13, 21050-21062, http://doi.org/10.1039/c1cp22478f, 2011.

Knopf, D. A., Poschl, U., and Shiraiwa, M.: Radial diffusion and penetration of gas molecules and aerosol particles through laminar flow reactors, denuders, and sampling tubes, Anal. Chem., 87, 3746-3754, http://doi.org/10.1021/ac5042395, 2015.

Knopf, D. A., Alpert, P. A., and Wang, B.: The Role of Organic Aerosol in Atmospheric Ice Nucleation: A Review, ACS Earth Space Chem., 2, 168-202, http://doi.org/10.1021/acsearthspacechem.7b00120, 2018.

Kolesar, K. R., Buffaloe, G., Wilson, K. R., and Cappa, C. D.: OH-initiated heterogeneous oxidation of internally-mixed squalane and secondary organic aerosol, Environ. Sci. Technol., 48, 3196-3202, http://doi.org/10.1021/es405177d, 2014.

Koop, T., Bookhold, J., Shiraiwa, M., and Poschl, U.: Glass transition and phase state of organic compounds: dependency on molecular properties and implications for secondary organic aerosols in the atmosphere, Phys. Chem. Chem. Phys., 13, 19238-19255, http://doi.org/10.1039/c1cp22617g, 2011.

Kroll, J. H., Lim, C. Y., Kessler, S. H., and Wilson, K. R.: Heterogeneous Oxidation of Atmospheric Organic Aerosol: Kinetics of Changes to the Amount and Oxidation State of Particle-Phase Organic Carbon, J. Phys. Chem. A, 119, 10767-10783, http://doi.org/10.1021/acs.jpca.5b06946, 2015.

Kwok, E., and Atkinson, R.: Estimation of hydroxyl radical reaction rate constants for gas-phase organic compounds using a structure-reactivity relationship: An update, Atmos. Environ., 29, 1685-1695, http://doi.org/10.1016/1352-2310(95)00069-b, 1995.

Laidler, K. J., Glasstone, S., and Eyring, H.: Application of the Theory of Absolute Reaction Rates to Heterogeneous Processes I. The Adsorption and Desorption of Gases, J. Chem. Phys., 8, 659-667, http://doi.org/10.1063/1.1750736, 1940.

Laskin, A., Laskin, J., and Nizkorodov, S. A.: Chemistry of atmospheric brown carbon, Chem. Rev., 115, 4335-4382, http://doi.org/10.1021/cr5006167, 2015.

Li, Z., Smith, K. A., and Cappa, C. D.: Influence of relative humidity on the heterogeneous oxidation of secondary organic aerosol, Atmos. Chem. Phys., 18, 14585-14608, http://doi.org/10.5194/acp-18-14585-2018, 2018.

Lienhard, D. M., Huisman, A. J., Krieger, U. K., Rudich, Y., Marcolli, C., Luo, B. P., Bones, D. L., Reid, J. P., Lambe, A. T., Canagaratna, M. R., Davidovits, P., Onasch, T. B., Worsnop, D. R., Steimer, S. S., Koop, T., and Peter, T.: Viscous organic aerosol particles in the upper troposphere: diffusivity-controlled water uptake and ice nucleation?, Atmos. Chem. Phys., 15, 13599-13613, http://doi.org/10.5194/acp-15-13599-2015, 2015.

Liu, Y., Ivanov, A. V., and Molina, M. J.: Temperature dependence of OH diffusion in air and He, Geophys. Res. Lett., 36, L03816, http://doi.org/10.1029/2008gl036170, 2009.

Marsh, A., Petters, S. S., Rothfuss, N. E., Rovelli, G., Song, Y. C., Reid, J. P., and Petters, M. D.: Amorphous phase state diagrams and viscosity of ternary aqueous organic/organic and inorganic/organic mixtures, Physical Chemistry Chemical Physics, 20, 15086-15097, 2018.

Marshall, F. H., Berkemeier, T., Shiraiwa, M., Nandy, L., Ohm, P. B., Dutcher, C. S., and Reid, J. P.: Influence of particle viscosity on mass transfer and heterogeneous ozonolysis kinetics in aqueous-sucrose-maleic acid aerosol, Phys. Chem. Chem. Phys., 20, 15560-15573, http://doi.org/10.1039/c8cp01666f, 2018.

Mason, E. A., and Monchick, L.: Transport Properties of Polar-Gas Mixtures, J. Chem. Phys., 36, 2746-2757, http://doi.org/10.1063/1.1732363, 1962.

McFiggans, G., Mentel, T. F., Wildt, J., Pullinen, I., Kang, S., Kleist, E., Schmitt, S., Springer, M., Tillmann, R., Wu, C., Zhao, D., Hallquist, M., Faxon, C., Le Breton, M., Hallquist, A. M., Simpson, D., Bergstrom, R., Jenkin, M. E., Ehn, M., Thornton, J. A., Alfarra, M. R., Bannan, T. J., Percival, C. J., Priestley, M., Topping, D., and Kiendler-Scharr, A.: Secondary organic aerosol reduced by mixture of atmospheric vapours, Nature, 565, 587-593, http://doi.org/10.1038/s41586-018-0871-y, 2019.

McNeill, V. F., Patterson, J., Wolfe, G. M., and Thornton, J. A.: The effect of varying levels of surfactant on the reactive uptake of N2O5 to aqueous aerosol, Atmos. Chem. Phys., 6, 1635-1644, http://doi.org/10.5194/acp-6-1635-2006, 2006.

Mellouki, A., Le Bras, G., and Sidebottom, H.: Kinetics and mechanisms of the oxidation of oxygenated organic compounds in the gas phase, Chem. Rev., 103, 5077-5096, http://doi.org/10.1021/cr020526x, 2003.

Mikhailov, E., Vlasenko, S., Martin, S. T., Koop, T., and Pöschl, U.: Amorphous and crystalline aerosol particles interacting with water vapor: conceptual framework and experimental evidence for restructuring, phase transitions and kinetic limitations, Atmos. Chem. Phys., 9, 9491-9522, http://doi.org/10.5194/acp-9-9491-2009, 2009.

Moise, T., and Rudich, Y.: Reactive uptake of ozone by proxies for organic aerosols: Surface versus bulk processes, J. Geophys. Res-Atmos., 105, 14667-14676, http://doi.org/10.1029/2000jd900071, 2000.

Moise, T., and Rudich, Y.: Uptake of Cl and Br by organic surfaces-A perspective on organic aerosols processing by tropospheric oxidants, Geophys. Res. Lett., 28, 4083-4086, http://doi.org/10.1029/2001gl013583, 2001.

Moise, T., and Rudich, Y.: Reactive Uptake of Ozone by Aerosol-Associated Unsaturated Fatty Acids: Kinetics, Mechanism, and Products, J. Phys. Chem. A, 106, 6469-6476, http://doi.org/10.1021/jp025597e, 2002.

Moise, T., Talukdar, R. K., Frost, G. J., Fox, R. W., and Rudich, Y.: Reactive uptake of NO3 by liquid and frozen organics, J. Geophys. Res-Atmos., 107, http://doi.org/10.1029/2001jd000334, 2002.

Moise, T., Flores, J. M., and Rudich, Y.: Optical properties of secondary organic aerosols and their changes by chemical processes, Chem. Rev., 115, 4400-4439, http://doi.org/10.1021/cr5005259, 2015.

Moridnejad, A., and Preston, T. C.: Models of Isotopic Water Diffusion in Spherical Aerosol Particles, J. Phys. Chem. A, 120, 9759-9766, http://doi.org/10.1021/acs.jpca.6b11241, 2016.

Mu, Q., Shiraiwa, M., Octaviani, M., Ma, N., Ding, A. J., Su, H., Lammel, G., Poschl, U., and Cheng, Y. F.: Temperature effect on phase state and reactivity controls atmospheric multiphase chemistry and transport of PAHs, Science Advances, 4, UNSP eaap7314, http://doi.org/10.1126/sciadv.aap7314, 2018.

Murphy, D. M., and Fahey, D. W.: Mathematical treatment of the wall loss of a trace species in denuder and catalytic converter tubes, Anal. Chem., 59, 2753-2759, http://doi.org/10.1021/ac00150a006, 1987.

Murray, B. J., Haddrell, A. E., Peppe, S., Davies, J. F., Reid, J. P., amp, apos, Sullivan, D., Price, H. C., Kumar, R., Saunders, R. W., Plane, J. M. C., Umo, N. S., and Wilson, T. W.: Glass formation and unusual hygroscopic growth of iodic acid solution droplets with relevance for iodine mediated particle formation in the marine boundary layer, Atmos. Chem. Phys., 12, 8575-8587, http://doi.org/10.5194/acp-12-8575-2012, 2012.

Nah, T., Kessler, S. H., Daumit, K. E., Kroll, J. H., Leone, S. R., and Wilson, K. R.: Influence of molecular structure and chemical functionality on the heterogeneous OH-initiated oxidation of unsaturated organic particles, J. Phys. Chem. A, 118, 4106-4119, http://doi.org/10.1021/jp502666g, 2014.

Orlando, J. J., Tyndall, G. S., and Ceazan, N.: Rate Coefficients and Product Yields from Reaction of OH with 1-Penten-3-ol, (Z)-2-Penten-1-ol, and Allyl Alcohol (2-Propen-1-ol), J. Phys. Chem. A, 105, 3564-3569, http://doi.org/10.1021/jp0041712, 2001.

Pachauri, R. K., Allen, M. R., Barros, V. R., Broome, J., Cramer, W., Christ, R., Church, J. A., Clarke, L., Dahe, Q., and Dasgupta, P.: Climate change 2014: synthesis report. Contribution of Working Groups I, II and III to the fifth assessment report of the Intergovernmental Panel on Climate Change, IPCC, Geneva, 151 pp., 2014.

Peterson, D. A., Campbell, J. R., Hyer, E. J., Fromm, M. D., Kablick, G. P., Cossuth, J. H., and DeLand, M. T.: Wildfire-driven thunderstorms cause a volcano-like stratospheric injection of smoke, NPJ Clim. Atmos. Sci., 1, 30, http://doi.org/10.1038/s41612-018-0039-3, 2018.

Petters, S. S., Kreidenweis, S. M., Grieshop, A. P., Ziemann, P. J., and Petters, M. D.: Temperature- and Humidity-Dependent Phase States of Secondary Organic Aerosols, Geophys. Res. Lett., 46, 1005-1013, http://doi.org/10.1029/2018gl080563, 2019.

Pöschl, U., Rudich, Y., and Ammann, M.: Kinetic model framework for aerosol and cloud surface chemistry and gas-particle interactions– Part 1: General equations, parameters, and terminology, Atmos. Chem. Phys., 7, 5989-6023, http://doi.org/acp-7-5989-2007, 2007.

Pöschl, U., and Shiraiwa, M.: Multiphase chemistry at the atmosphere-biosphere interface influencing climate and public health in the anthropocene, Chem. Rev., 115, 4440-4475, http://doi.org/10.1021/cr500487s, 2015.

Price, H. C., Mattsson, J., Zhang, Y., Bertram, A. K., Davies, J. F., Grayson, J. W., Martin, S. T., O'Sullivan, D., Reid, J. P., Rickards, A. M. J., and Murray, B. J.: Water diffusion in atmospherically relevant alpha-pinene secondary organic material, Chem. Sci., 6, 4876-4883, http://doi.org/10.1039/c5sc00685f, 2015.

Reid, J. P., Bertram, A. K., Topping, D. O., Laskin, A., Martin, S. T., Petters, M. D., Pope, F. D., and Rovelli, G.: The viscosity of atmospherically relevant organic particles, Nat. Commun., 9, 956, http://doi.org/10.1038/s41467-018-03027-z, 2018.

Renbaum-Wolff, L., Grayson, J. W., Bateman, A. P., Kuwata, M., Sellier, M., Murray, B. J., Shilling, J. E., Martin, S. T., and Bertram, A. K.: Viscosity of alpha-pinene secondary organic material and implications for particle growth and reactivity, Proc. Nat. Acad. Sci. U.S.A., 110, 8014-8019, http://doi.org/10.1073/pnas.1219548110, 2013.

Ribeiro, L. M., Viegas, D. X., Almeida, M., McGee, T. K., Pereira, M. G., Parente, J., Xanthopoulos, G., Leone, V., Delogu, G. M., and Hardin, H.: Extreme wildfires and disasters around the world, in: Extreme Wildfire Events and Disasters, Elsevier, 31-51, http://doi.org/10.1016/b978-0-12-815721-3.00002-3, 2020.

Riemer, N., Ault, A. P., West, M., Craig, R. L., and Curtis, J. H.: Aerosol Mixing State: Measurements, Modeling, and Impacts, Rev. Geophys., 57, 187-249, http://doi.org/10.1029/2018rg000615, 2019.

Robinson, A. L., Subramanian, R., Donahue, N. M., Bernardo-Bricker, A., and Rogge, W. F.: Source apportionment of molecular markers and organic aerosol. 2. Biomass smoke, Environ. Sci. Technol., 40, 7811-7819, http://doi.org/10.1021/es060782h, 2006.

Robinson, A. L., Donahue, N. M., Shrivastava, M. K., Weitkamp, E. A., Sage, A. M., Grieshop, A. P., Lane, T. E., Pierce, J. R., and Pandis, S. N.: Rethinking organic aerosols: semivolatile emissions and photochemical aging, Science, 315, 1259-1262, http://doi.org/10.1126/science.1133061, 2007.

Rogers, D. F.: Laminar flow analysis, Cambridge University Press, Edinburgh Building, Cambridge, 422 pp., 1992.

Rosenhead, L.: Laminar boundary layers, Dover, New York, 687 pp., 1988.

Rothfuss, N. E., and Petters, M. D.: Characterization of the temperature and humidity-dependent phase diagram of amorphous nanoscale organic aerosols, Phys. Chem. Chem. Phys., 19, 6532-6545, http://doi.org/10.1039/c6cp08593h, 2017.

Rudich, Y., Talukdar, R. K., Imamura, T., Fox, R. W., and Ravishankara, A. R.: Uptake of NO3 on KI solutions: rate coefficient for the NO3 + I− reaction and gas-phase diffusion coefficients for NO3, Chem. Phys. Lett., 261, 467-473, http://doi.org/10.1016/0009-2614(96)00980-3, 1996.

Rudich, Y., Donahue, N. M., and Mentel, T. F.: Aging of organic aerosol: bridging the gap between laboratory and field studies, Annu. Rev. Phys. Chem., 58, 321-352, http://doi.org/10.1146/annurev.physchem.58.032806.104432, 2007.

Schröter, K., and Donth, E.: Viscosity and shear response at the dynamic glass transition of glycerol, J. Chem. Phys., 113, 9101-9108, http://doi.org/10.1063/1.1319616, 2000.

Schwartz, S. E.: Mass-transport considerations pertinent to aqueous phase reactions of gases in liquid-water clouds, in: Chemistry of multiphase atmospheric systems, Springer, Berlin, Heidelberg, Germany, 415-471, http://doi.org/10.1007/978-3-642-70627-1, 1986.

Seinfeld, J. H., and Pandis, S. N.: Atmospheric chemistry and physics: from air pollution to climate change, 3rd ed., John Wiley & Sons, Hoboken, New Jersey, 1152 pp., 2016.

Shiraiwa, M., Garland, R. M., and Pöschl, U.: Kinetic double-layer model of aerosol surface chemistry and gas-particle interactions (K2-SURF): Degradation of polycyclic aromatic hydrocarbons exposed to O3, NO2, H2O, OH and NO3, Atmos. Chem. Phys., 9, 9571-9586, http://doi.org/10.5194/acp-9-9571-2009, 2009.

Shiraiwa, M., Pfrang, C., and Pöschl, U.: Kinetic multi-layer model of aerosol surface and bulk chemistry (KM-SUB): the influence of interfacial transport and bulk diffusion on the oxidation of oleic acid by ozone, Atmos. Chem. Phys., 10, 3673-3691, http://doi.org/10.5194/acp-10-3673-2010, 2010.

Shiraiwa, M., Ammann, M., Koop, T., and Poschl, U.: Gas uptake and chemical aging of semisolid organic aerosol particles, Proc. Nat. Acad. Sci. U.S.A., 108, 11003-11008, http://doi.org/10.1073/pnas.1103045108, 2011.

Shiraiwa, M., Poschl, U., and Knopf, D. A.: Multiphase Chemical Kinetics of NO3 Radicals Reacting with Organic Aerosol Components from Biomass Burning, Environ. Sci. Technol., 46, 6630-6636, http://doi.org/10.1021/es300677a, 2012.

Shiraiwa, M., and Seinfeld, J. H.: Equilibration timescale of atmospheric secondary organic aerosol partitioning, Geophys. Res. Lett., 39, L24801 http://doi.org/10.1029/2012gl054008, 2012.

Shiraiwa, M., Li, Y., Tsimpidi, A. P., Karydis, V. A., Berkemeier, T., Pandis, S. N., Lelieveld, J., Koop, T., and Poschl, U.: Global distribution of particle phase state in atmospheric secondary organic aerosols, Nat. Commun., 8, 15002, http://doi.org/10.1038/ncomms15002, 2017a.

Shiraiwa, M., Ueda, K., Pozzer, A., Lammel, G., Kampf, C. J., Fushimi, A., Enami, S., Arangio, A. M., Frohlich-Nowoisky, J., Fujitani, Y., Furuyama, A., Lakey, P. S. J., Lelieveld, J., Lucas, K., Morino, Y., Poschl, U., Takaharna, S., Takami, A., Tong, H. J., Weber, B., Yoshino, A., and Sato, K.: Aerosol Health Effects from Molecular to Global Scales, Environ. Sci. Technol., 51, 13545-13567, http://doi.org/10.1021/acs.est.7b04417, 2017b.

Slade, J. H., and Knopf, D. A.: Heterogeneous OH oxidation of biomass burning organic aerosol surrogate compounds: assessment of volatilisation products and the role of OH concentration on the reactive uptake kinetics, Phys. Chem. Chem. Phys., 15, 5898-5915, http://doi.org/10.1039/c3cp44695f, 2013.

Slade, J. H., and Knopf, D. A.: Multiphase OH oxidation kinetics of organic aerosol: The role of particle phase state and relative humidity, Geophys. Res. Lett., 41, 5297-5306, http://doi.org/10.1002/2014gl060582, 2014.

Slade, J. H., Shiraiwa, M., Arangio, A., Su, H., Pöschl, U., Wang, J., and Knopf, D. A.: Cloud droplet activation through oxidation of organic aerosol influenced by temperature and particle phase state, Geophys. Res. Lett., 44, 1583-1591, http://doi.org/10.1002/2016gl072424, 2017.

Springmann, M., Knopf, D. A., and Riemer, N.: Detailed heterogeneous chemistry in an urban plume box model: reversible co-adsorption of O3, NO2, and H2O on soot coated with benzo[a]pyrene, Atmos. Chem. Phys., 9, 7461-7479, http://doi.org/10.5194/acp-9-7461-2009, 2009.

Steimer, S. S., Berkemeier, T., Gilgen, A., Krieger, U. K., Peter, T., Shiraiwa, M., and Ammann, M.: Shikimic acid ozonolysis kinetics of the transition from liquid aqueous solution to highly viscous glass, Phys. Chem. Chem. Phys., 17, 31101-31109, http://doi.org/10.1039/c5cp04544d, 2015.

Virtanen, A., Joutsensaari, J., Koop, T., Kannosto, J., Yli-Pirila, P., Leskinen, J., Makela, J. M., Holopainen, J. K., Poschl, U., Kulmala, M., Worsnop, D. R., and Laaksonen, A.: An amorphous solid state of biogenic secondary organic aerosol particles, Nature, 467, 824-827, http://doi.org/10.1038/nature09455, 2010.

Wallace, J. M., and Hobbs, P. V.: Atmospheric science: an introductory survey, 2nd ed., Elsevier, 504 pp., 2006.

Waring, C., King, K. L., Bagot, P. A., Costen, M. L., and McKendrick, K. G.: Collision dynamics and reactive uptake of OH radicals at liquid surfaces of atmospheric interest, Phys. Chem. Chem. Phys., 13, 8457-8469, http://doi.org/10.1039/C0CP02734K, 2011.

Wutz, M.: Theory and practice of vacuum technology, Vieweg, Braunschweig, Germany, 667 pp., 1989.

Yang, Z., Liu, X., Yang, Z., Zhuang, G., Bai, Z., Zhang, H., and Guo, Y.: Preparation and formation mechanism of levoglucosan from starch using a tubular furnace pyrolysis reactor, J. Anal. Appl. Pyrol., 102, 83-88, http://doi.org/10.1016/j.jaap.2013.03.012, 2013.

Zasypkin, A. Y., Grigor'eva, V. M., Korchak, V. N., and Gershenson, Y. M.: A formula for summing of kinetic resistances for mobile and stationary media: I. Cylindrical reactor, Kinet. Catal+. 38, 772-781, 1997.

Zhou, S., Hwang, B. C. H., Lakey, P. S. J., Zuend, A., Abbatt, J. P. D., and Shiraiwa, M.: Multiphase reactivity of polycyclic aromatic hydrocarbons is driven by phase separation and diffusion limitations, Proc. Nat. Acad. Sci. U.S.A., 116, 11658-11663, http://doi.org/10.1073/pnas.1902517116, 2019.

Ziemann, P. J.: Aerosol products, mechanisms, and kinetics of heterogeneous reactions of ozone with oleic acid in pure and mixed particles, Faraday Discuss., 130, 469-490, http://doi.org/10.1039/b417502f, 2005.

Zobrist, B., Marcolli, C., Pedernera, D. A., and Koop, T.: Do atmospheric aerosols form glasses?, Atmos. Chem. Phys., 8, 5221-5244, http://doi.org/10.5194/acp-8-5221-2008, 2008.

Zobrist, B., Soonsin, V., Luo, B. P., Krieger, U. K., Marcolli, C., Peter, T., and Koop, T.: Ultra-slow water diffusion in aqueous sucrose glasses, Phys. Chem. Chem. Phys., 13, 3514-3526, http://doi.org/10.1039/c0cp01273d, 2011.

905

Table 1. Estimated T_g of the applied film substrates. T_g^{exp} is the measured T_g using the poke-flow technique. T_g^{lit} is the literature reported T_g. T_g^{pred} is predicted T_g for mixtures by Gordon-Taylor equation using T_g^{lit} and k_{GT}. k_{GT} is solute specific constant in the Gordon-Taylor equation. D is fragility.

Substrate	T_g^{exp} / K	T_g^{pred} / K	T_g^{lit} / K	k_{GT}	D
Levoglucosan (LEV)	243 ± 4		249[a]	3.26[a]	14.1[b]
Xylitol (XYL)			247[c]	2.1[c]	8.65[b]
LEV/XYL	238 ± 3	248			11.3[d]
Glucose (GLU)	273 ± 3		296[e]	3.95[e]	12.1[b]
1,2,6-Hexanetriol (HEX)			202[f]	0.88[e]	13.16[f]
GLU/HEX	248 ± 3	246			12.3[d]

[a] Lienhard et al. (2012). [b]DeRieux et al. (2018). [c]Elamin et al. (2012). [d] Interpolated values based on mass fraction. [e]Zobrist et al. (2008). [f] Nakanishi et al. (2011).

910

915

920

925

Table 2. Comparison of uptake coefficients of NO_3 on liquid and solid substrates of saturated and unsaturated organics.

Surface	Liquid surface		Solid surface	
	T / K	γ_{liquid}	T / K	γ_{solid}
LEV			293	$(4.2\pm0.6)\times10^{-4a}$
LEV			213	$(2.8\pm0.3)\times10^{-4a}$
LEV/XYL	293	$(8\pm2)\times10^{-4a}$	213	$(3.10\pm0.9)\times10^{-4a}$
Glycerol	293	$(1.4\pm0.3)\times10^{-3b}$		
Glycerol	268	$(8.3\pm0.5)\times10^{-4b}$		
1-octanol	258	$(7.1\pm1.6)\times10^{-3c}$	248	$(4.1\pm1.0)\times10^{-3c}$
DES	298	$(4.1\pm0.3)\times10^{-3b}$	263	$(2.5\pm0.2)\times10^{-4b}$
n-Hexadecane	293	$(2.6\pm0.8)\times10^{-3c}$	283-289	$(3.8\pm1.0)\times10^{-4c}$

[a]This study. [b]Gross et al. (2009). [c]Moise et al. (2002).

930

935

940

945
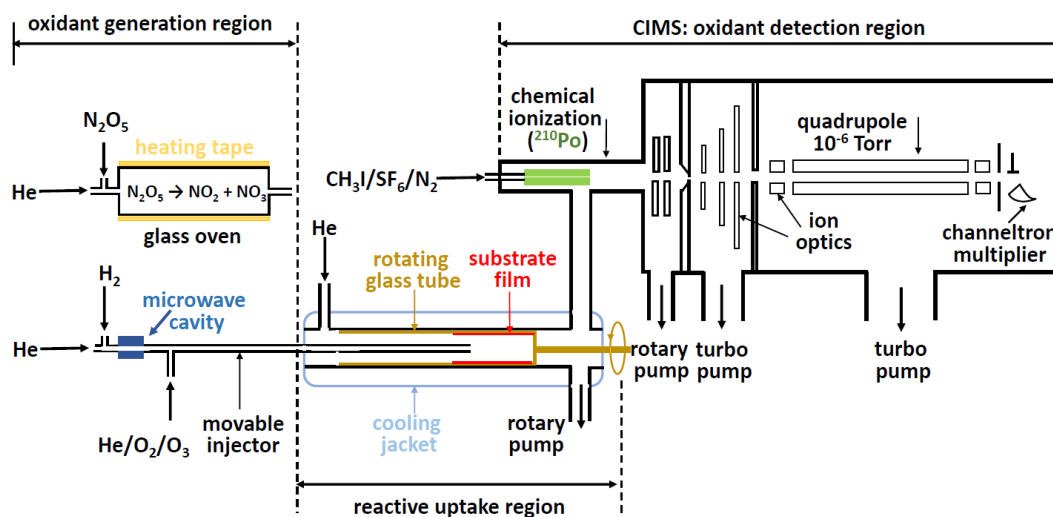
Figure 1: Schematic of the low-temperature coated-wall flow reactor coupled to the chemical ionization mass spectrometer (CIMS). The oxidant generation region displays the generation methods for NO₃ and OH radicals.

950

955

960

965

970
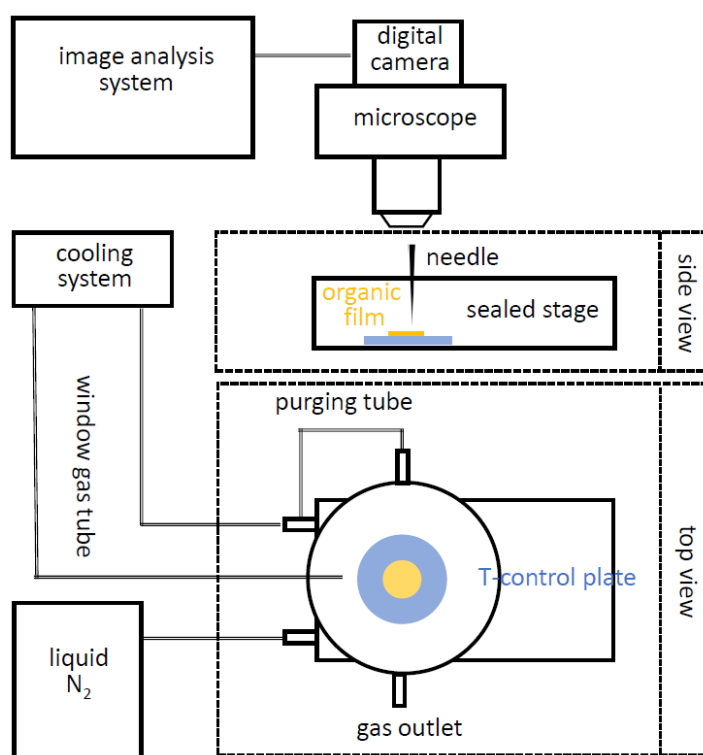
Figure 2. Schematic of the experimental poke-flow setup. This includes a temperature controlled Linkam cooling stage coupled to a microscope equipped with a digital camera and an image analysis system.

975

980
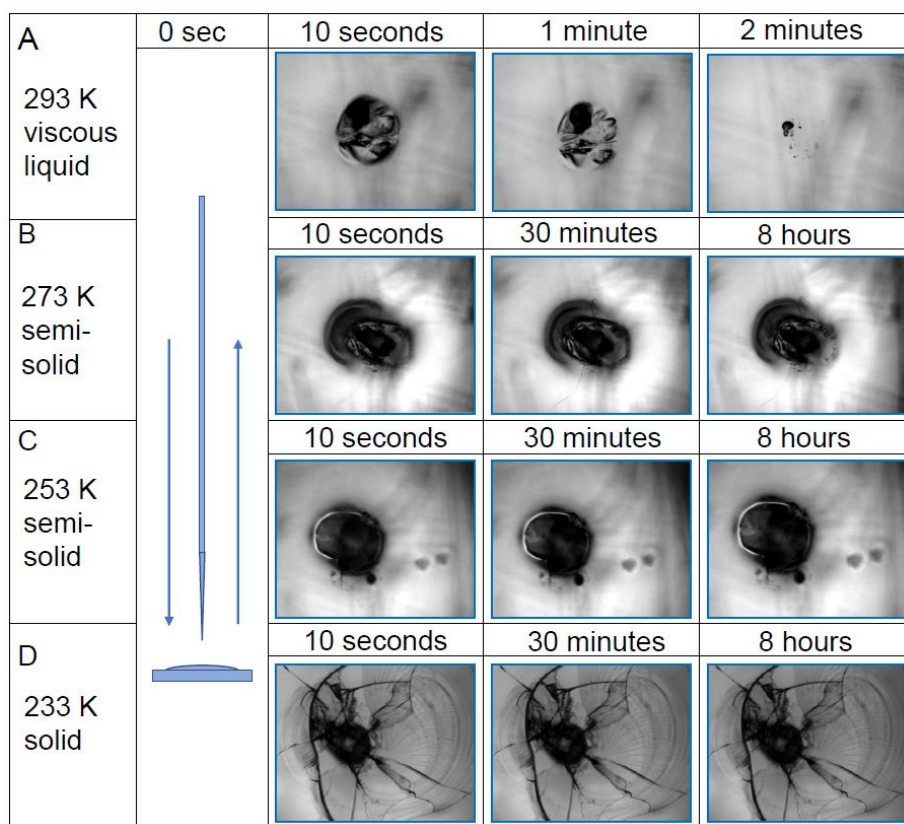
Figure 3. Estimation of the phase state of the film substrate as shown for a GLU/HEX mixture (mass ratio of 4:1). Deformation and recovery were monitored for different time periods due to the poking of the substrate at different temperatures. The microscope images are 200 µm wide.

985

990

995
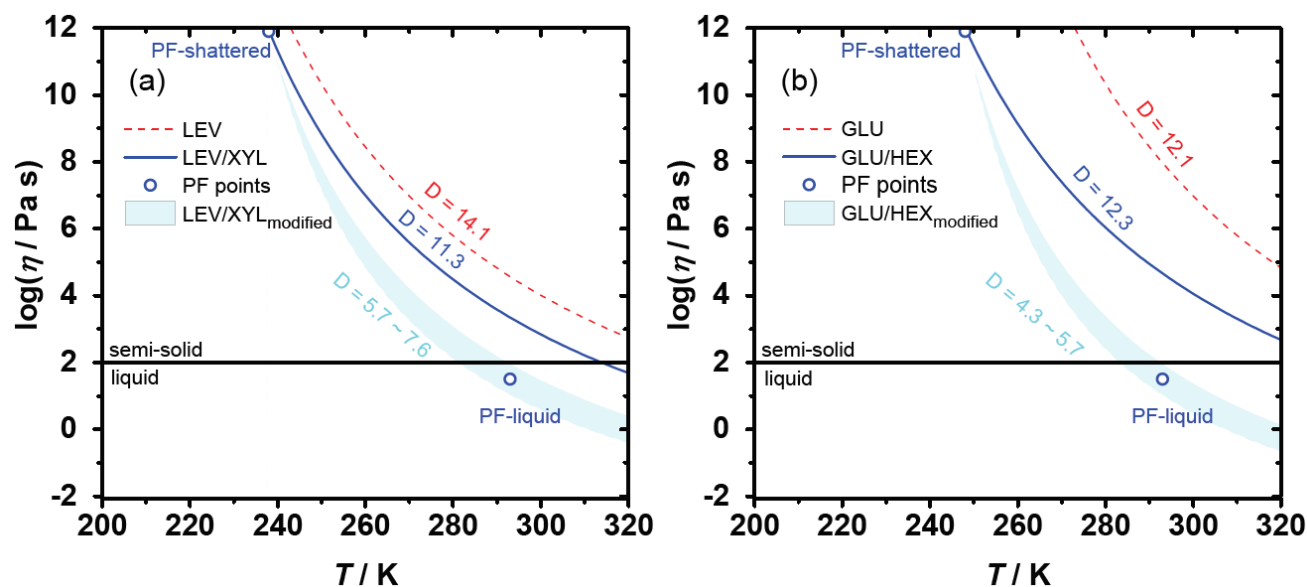
Figure 4. The Angell plot of viscosity as a function of temperature for LEV, LEV/XYL, GLU and GLU/HEX substrates. The lines represent predicted viscosities as a function of T_g^{exp} and applied D values (see Table 1). PF-shattered and PF-liquid (blue circles) indicate the conditions for which the poke-flow (PF) experiment detected a solid (glassy) and liquid phase state of the substrate, respectively. The shaded areas represent predicted viscosities by using the VTF equation with modified D values as indicated in the panels based on the estimated viscosities derived from the poke-flow experiment. The horizontal black line at $\eta = 10^2$ Pa s indicates the threshold of liquid and semi-solid phase states.

1000

1005

1010
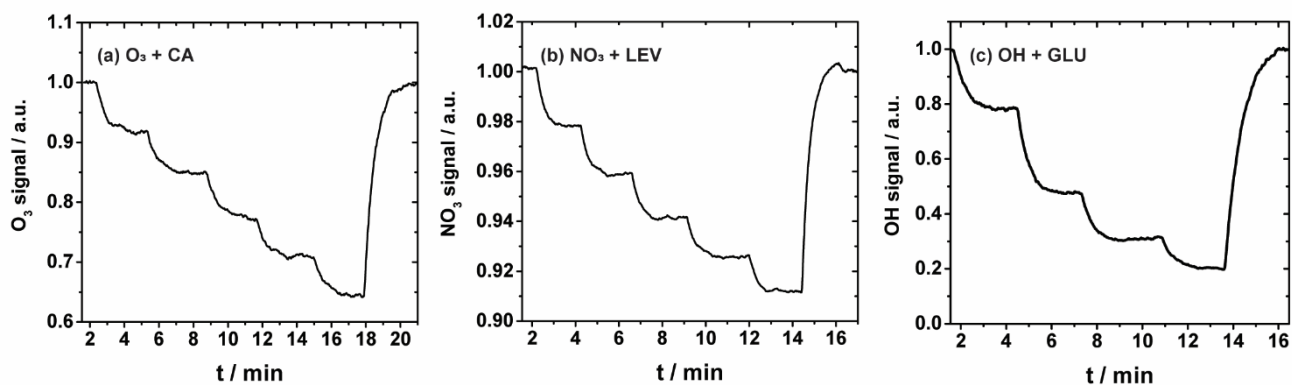
Figure 5. Reactive uptake experiments showing the change in the normalized gas-phase oxidant signal as the reaction time is changed by pulling back the injector incrementally. (a) uptake of O_3 by canola oil (CA); (b) uptake of NO_3 by levoglucosan (LEV); (c) uptake of OH radical by glucose (GLU).

1015

1020

1025

1030

1035
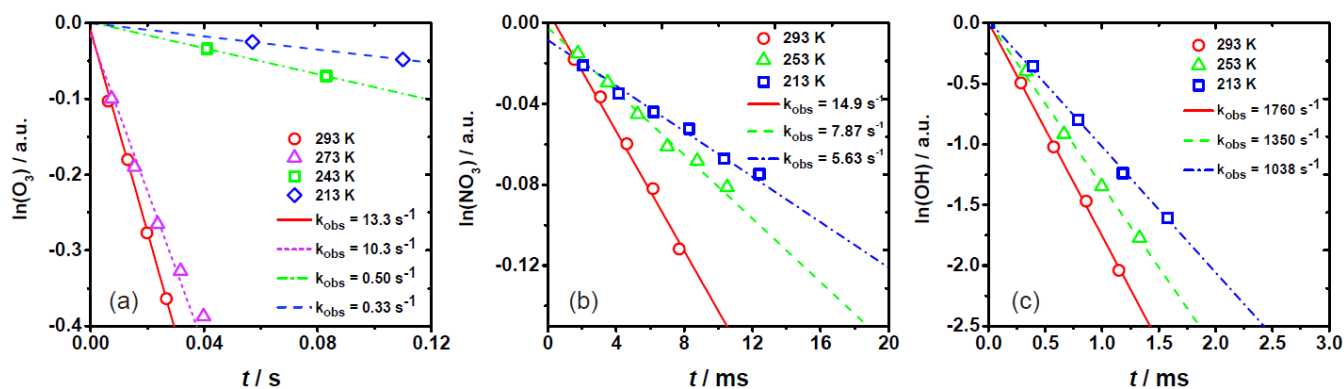
Figure 6. Natural logarithm of the change in gas-phase oxidant signal as a function of reaction time for (a) O_3 uptake by CA, (b) NO_3 uptake by LEV/XYL mixture, and (c) OH uptake by GLU/HEX mixture. Open circles, triangles, squares, and diamonds correspond to uptake measurements at different temperatures. Lines represent the corresponding linear fits to the data and corresponding slopes. k_{obs} values are given in legend.

1040

1045

1050

1055
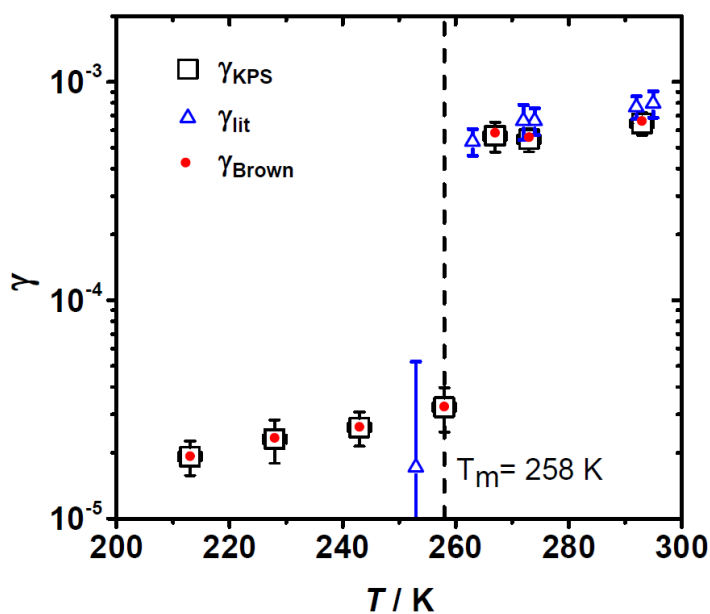
Figure 7. Reactive uptake coefficients of O₃ by canola oil as a function of temperature. Squares and red circles represent γ values derived using the KPS and Brown method, respectively. See text for more details. γ_{lit} represents values reported by de Gouw et al. (1998).

1060

1065
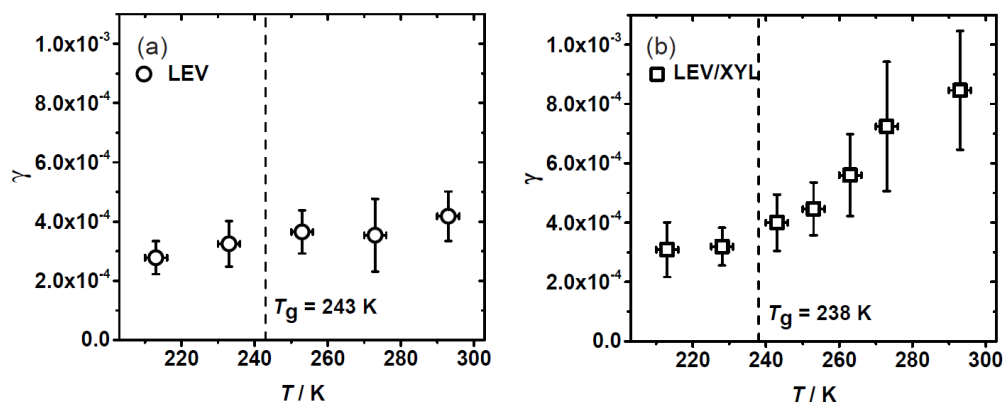
Figure 8. Reactive uptake coefficients, γ, of NO₃ reacting with (a) levoglucosan (LEV) and (b) 1:1 by mass LEV and xylitol (XYL) mixture as a function of temperature. The dashed line represents the glass transition temperature (T_g) measured in the poke-flow experiment.

1090
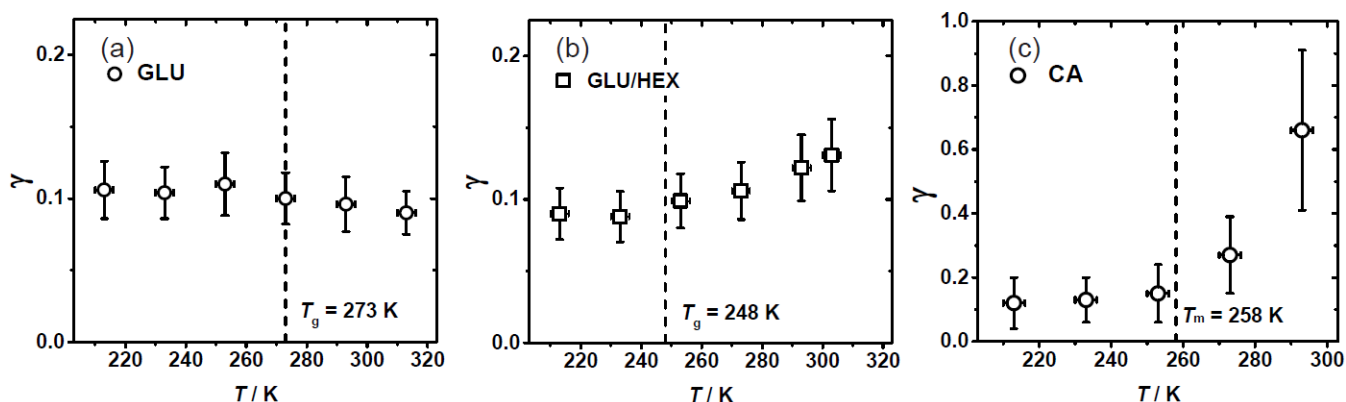
Figure 9. Reactive uptake coefficients, γ, of OH radicals reacting with (a) glucose (GLU), (b) 1:4 by mass glucose and 1,2,6-hexanetriol (GLU/HEX) mixture and (c) canola oil (CA) as a function of temperature. T_g is the glass transition temperature determined in the poke-flow experiment.

1095

1100

1105

1110

1115
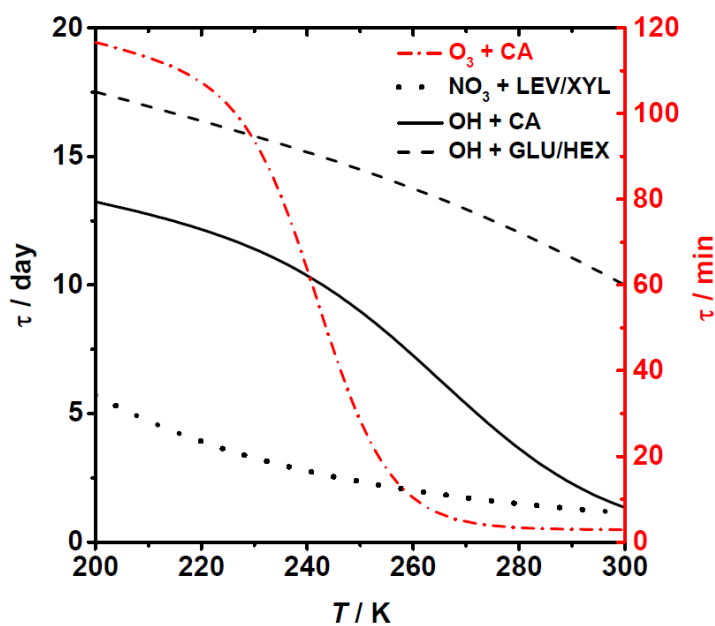
Figure 10. Lifetime estimates of one monolayer of examined OA surrogates for typical background concentrations of O_3, NO_3, and OH. See text for more details.

1120

1125

1130

1135
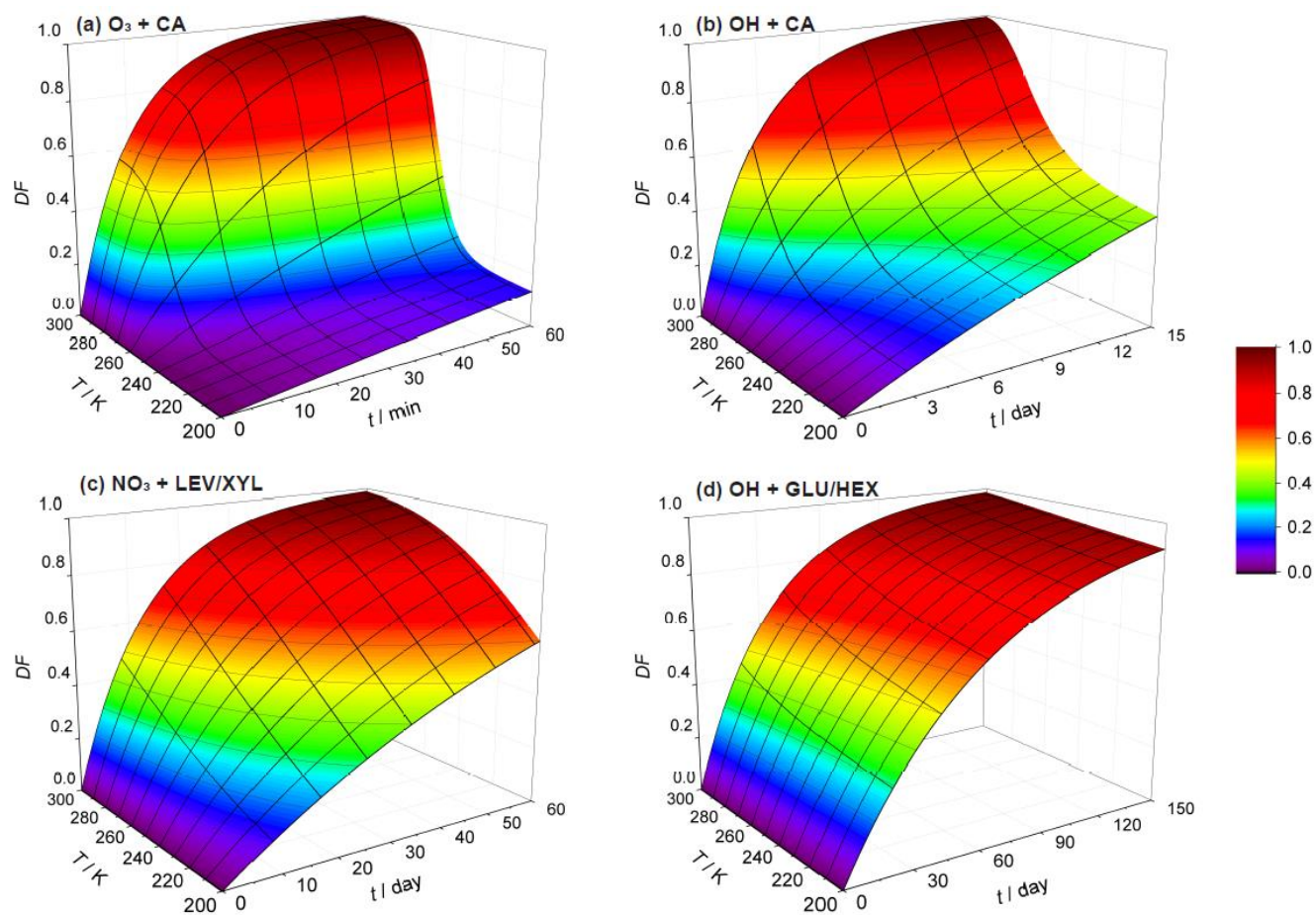
Figure 11. Exposure and temperature dependent particle degraded fraction (DF) for particles 200 nm in diameter for (a) O₃ oxidation of canola oil, (b) OH oxidation of canola oil, (c) NO₃ oxidation of LEV/XYL mixture, and (d) OH oxidation of GLU/HEX mixture. Note the different scales on the time axis.

1140

1145
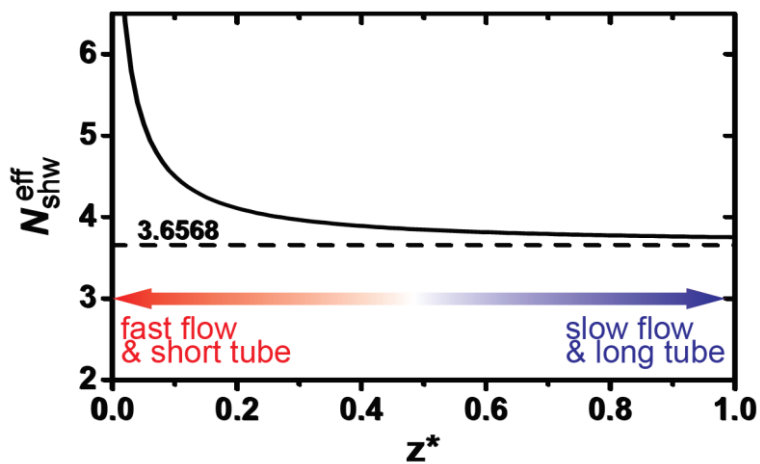
Figure A1. Dependence of the effective Sherwood number (N_{shw}^{eff}) on the dimensionless axial distance of the flow reactor. Smaller dimensionless axial distance represents the scenario of a fast flow or short tube. Adapted from Davies (2008) and Knopf et al. (2015).

1150

1155

1160

1165
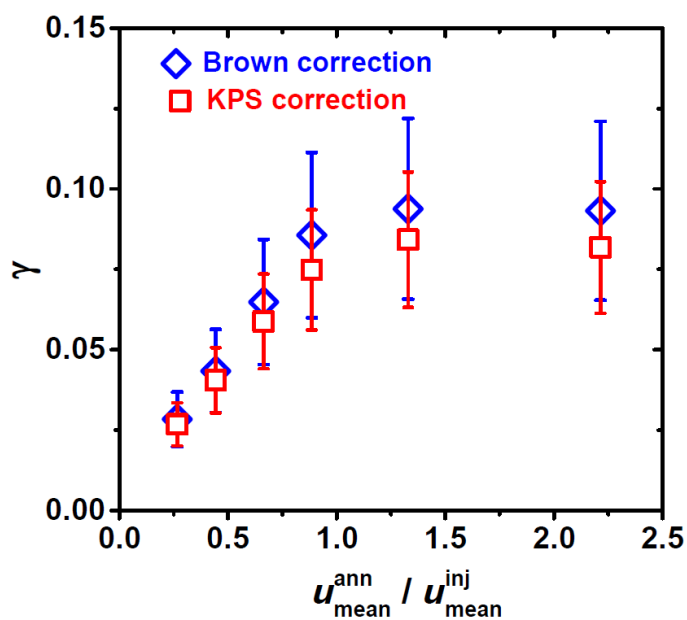
Figure A2. Differences in reactive uptake coefficient (γ) derived from two gas transport correction methods for fast heterogeneous kinetics involving OH uptake by glucose as a function of flow velocity ratio between mean gas flow velocity in the annular section of the flow reactor (u_{mean}^{ann}) and the gas flow exiting the movable injector (u_{mean}^{inj}). Red squares and blue diamonds represent KPS and Brown methods, respectively.

1170